JOURNAL OF GEOPHYSICAL RESEARCH, VOL. 113, B03307, doi:10.1029/2007JB005113, 2008

Seismic structure of the southern Gulf of California from Los Cabos block to the East Pacific Rise

P. Páramo,[1,2] W. S. Holbrook,[1] H. E. Brown,[1] D. Lizarralde,[3] J. Fletcher,[4] P. Umhoefer,[5] G. Kent,[6] A. Harding,[6] A. Gonzalez,[4] and G. Axen[7]

Received 1 April 2007; revised 9 September 2007; accepted 25 October 2007; published 15 March 2008.

[1] Multichannel reflection and coincident wide-angle seismic data collected during the 2002 Premier Experiment, Sea of Cortez, Addressing the Development of Oblique Rifting (PESCADOR) experiment provide the most detailed seismic structure to date of the southern Gulf of California. Multichannel seismic (MCS) data were recorded with a 6-km-long streamer, 480-channel, aboard the R/V *Maurice Ewing*, and wide-angle data was recorded by 19 instruments spaced every ~12 km along the transect. The MCS and wide-angle data reveal the seismic structure across the continent-ocean transition of the rifted margin. Typical continental and oceanic crust are separated by a ~75-km-wide zone of extended continental crust dominated by block-faulted basement. Little lateral variation in crustal thicknesses and seismic velocities is observed in the oceanic crust, suggesting a constant rate of magmatic productivity since seafloor spreading began. Oceanic crustal thickness and mean crustal velocities suggest normal mantle temperature (1300°C) and passive mantle upwelling at the early stages of seafloor spreading. The crustal thickness, width of extended continental crust, and predicted temperature conditions all indicate a narrow rift mode of extension. On the basis of upper and lower crust stretching factors, an excess of lower crust was found in the extended continental crust. Total extension along transect 5W is estimated to be ~35 km. Following crustal extension, new oceanic crust ~6.4-km-thick was formed at a rate of ~48 mm a^{-1} to accommodate plate separation.

Citation: Páramo, P., W. S. Holbrook, H. E. Brown, D. Lizarralde, J. Fletcher, P. Umhoefer, G. Kent, A. Harding, A. Gonzalez, and G. Axen (2008), Seismic structure of the southern Gulf of California from Los Cabos block to the East Pacific Rise, *J. Geophys. Res.*, *113*, B03307, doi:10.1029/2007JB005113.

1. Introduction

[2] Continental rupture is an important process affected by magmatism and tectonic deformation. Many fundamental questions remain unsolved about the way the lithosphere behaves during continental breakup and the effect on rift evolution of key parameters such as crustal thickness, spreading rate, composition, and temperature.

[3] Continental extension begins when tensional stress is applied to the crust until the lithosphere breaks apart, culminating in lithospheric rupture and the creation of new oceanic lithosphere to accommodate plate separation. Two end-member models have been suggested to describe how the crust deforms and extends: pure shear [*McKenzie*, 1978], where the same amount of extension is applied to the upper and lower crust, generally producing symmetric margins, and simple shear [*Lister et al.*, 1986], where a low-angle shear zone extends through the entire lithosphere, distributing thinning of the crust and lithosphere differential and necessarily producing asymmetric margins. Combinations of these end-member mechanisms can produce a variety of rift structures [*Buck*, 1991; *Kusznir et al.*, 1991; *Bassi et al.*, 1993]. Continental rifts can develop by strain localization as a consequence of simple plastic deformation or a more complex pattern of brittle layers [e.g., *Dunbar and Sawyer*, 1989]. Lithospheric necking can proceed to rupture with or without lower crustal flow, which might affect crustal thinning profiles [*Hopper and Buck*, 1996]. Continental breakup is a complex process distributed in time and space [*Péron-Pinvidic et al.*, 2007] and other forms of depth-dependent stretching besides simple shear have been suggested to explain the evolution of deformation during extension of the continental lithosphere [*Davis and Kusznir*, 2004; *Lavier and Manatschal*, 2006].

[4] Continental rifts are typically classified morphologically between narrow and wide rift end-members, with no

[1]Department of Geology and Geophysics, University of Wyoming, Laramie, Wyoming, USA.
[2]Now at BP Exploration Operating Company Ltd., Sunbury-on-Thames, UK.
[3]Department of Geology and Geophysics, Woods Hole Oceanographic Institution, Woods Hole, Massachusetts, USA.
[4]Department of Geology, Centro de Investigación Científica y de Educación Superior de Ensenada, Ensenada, Baja California, Mexico.
[5]Department of Geology, Northern Arizona University, Flagstaff, Arizona, USA.
[6]Scripps Institution of Oceanography, University of California, San Diego, La Jolla, California, USA.
[7]Department of Earth and Environmental Science, New Mexico Institute of Mining and Technology, Socorro, New Mexico, USA.

0148-0227/08/2007JB005113$09.00

direct correlation between pure and simple shear styles of extension. Numerical models have defined conditions under which narrow and wide rifts develop [e.g., *Buck*, 1991]. Narrow rifts, such as the East Africa Rift and Gulf of Suez, may form where the crust was originally cold and thin (~30 km) and are characterized by ~100-km-wide region of intense normal faulting and strong lateral gradients in crustal thickness; wide rifts, such as the Basin and Range Province, have a more distributed deformation and may form where the crust was originally warm and thick (>40 km) [*Buck*, 1991; *Bassi*, 1995; *Hopper and Buck*, 1996].

[5] Rift-related magmatism is principally controlled by mantle temperature, rate and duration of extension, and the initial lithospheric thickness [e.g., *Bown and White*, 1994]. Rifted margins can be magmatically classified based on crustal seismic observations. Volcanic margins are generally characterized by sections of igneous rocks more than twice as thick as normal oceanic crust, with higher-than-normal lower crustal velocities [*White and McKenzie*, 1989; *Holbrook and Kelemen*, 1993; *Holbrook et al.*, 1994] and seaward dipping reflectors created by extrusive igneous bodies [*Mutter et al.*, 1982]. Volcanic margins are commonly associated with high mantle temperature anomalies [*White and McKenzie*, 1989; *Holbrook et al.*, 2001] allowing significant melt to form under extension. Nonvolcanic margins, in contrast, are characterized by little magmatism, a block-faulted basement, and, in some cases, exhumed mantle (serpentinized peridotite), and they typically lack an abrupt boundary between thinned continental crust and typical oceanic crust [e.g., *Pinheiro et al.*, 1992; *Chian et al.*, 1995; *Dean et al.*, 2000; *Pérez-Gussinyé and Reston*, 2001; *Funck et al.*, 2003; *Pérez-Gussinyé et al.*, 2003]. However, the transition between the unextended continental crust and typical oceanic crust across nonvolcanic margins does appear to have a distinct velocity structure consisting of a thin upper layer (<3 km thick) with velocities between ~4.0 km s^{-1} at the top and ~6.5 km s^{-1} at the bottom of the layer, and a high-velocity deeper layer (~7.5 km s^{-1}) [e.g., *Pinheiro et al.*, 1992; *Chian and Louden*, 1995; *Chian et al.*, 1995; *Dean et al.*, 2000; *Funck et al.*, 2003]. These observed deep, high-velocity layers have been interpreted as serpentinized peridotite in the Labrador Sea [*Chian et al.*, 1995], the Newfoundland [*Reid*, 1994] and west Iberia margins [*Whitmarsh and Sawyer*, 1996; *Pickup et al.*, 1996], and the Otway Basin in southeast Australia [*Finlayson et al.*, 1998]. For all these margins, distances between unextended continental crust and normal oceanic crust typically vary between ~100 and 200 km. The limited magmatism of these nonvolcanic margins has been attributed to ultraslow spreading and cold mantle temperature conditions, where conductive heat loss suppressed melt generation.

[6] Crustal-scale observations are needed to improve understanding of rifting processes. Seismic structure obtained from multichannel seismic (MCS) and wide-angle data has provided crucial information about the evolution of rifted margins such as patterns of crustal extension [*Chian and Louden*, 1995; *Dean et al.*, 2000; *Funck et al.*, 2003; *Pérez-Gussinyé et al.*, 2003; *González-Fernández et al.*, 2005], distribution of magmatic material [e.g., *Holbrook et al.*, 1994], and estimates of mantle temperature and upwelling ratios [*Holbrook et al.*, 2001; *Korenaga et al.*, 2002; *Sallares et al.*, 2003; *Sallares and Charvis*, 2003]. In this study we present MCS and coincident wide-angle data that image structures produced during the rift-to-drift evolution of the southern Gulf of California. Stacked MCS seismic sections show clear images of faults and basement structure along the transect. Wide-angle data provide a crustal-scale velocity model across the continent-ocean transition. The data were collected in the fall of 2002 during the Premier Experiment, Sea of Cortez, Addressing the Development of Oblique Rifting (PESCADOR) experiment. Data from the conjugate margin are being processed independently and will be presented in future work [*Brown et al.*, 2005].

2. Gulf of California

[7] Continental rupture in the Gulf Extensional Province (GEP) took place mainly in two phases: (1) The protogulf, a period of continental rifting dominated by NNW striking normal faults [*Karig and Jensky*, 1972; *Oskin et al.*, 2001], when the first marine basins were produced, and (2) a later regime of strike-slip, extension, and seafloor spreading [*Karig and Jensky*, 1972]. The transitional period between these phases is believed to have initiated ~8 Ma [*Atwater and Stock*, 1998; *Axen et al.*, 2000] and concluded with the formation of new oceanic crust ~3.6 Ma [*Lonsdale*, 1989; *Umhoefer et al.*, 1994].

[8] Prior to ~29 Ma, the Farallon plate was being subducted beneath the west margin of what is now the Baja California Peninsula [*Atwater*, 1970]. As the East Pacific Rise, separating the Pacific and Farallon plates, approached the paleotrench, the Farallon plate split into a number of microplates that, as spreading at the ridges of those microplates stalled [*Michaud et al.*, 2006], became part of the Pacific plate. With this plate reorganization, subduction stalled, shutting down arc volcanism progressively from north (~16 Ma) to south (~11 Ma) [*Sawlan*, 1991; *Stock and Lee*, 1994] and resulting in the coupling of the present-day Baja Peninsula to the Pacific plate and the onset of localized rifting in the Gulf of California. *Axen et al.* [2000] suggested that significant oblique rifting characterized the Gulf since at least ~8 Ma. Extension continued with the creation and development of transform faults and pull-apart basins from ~8 Ma to ~3.6 Ma, until the peninsula of Baja California was attached to the Pacific plate [*Lonsdale*, 1989; *Dixon et al.*, 2000]. Spreading has averaged ~48 mm a^{-1} since ~3.6 Ma [*DeMets et al.*, 1987], and at present, the Baja California Peninsula moves nearly completely with the Pacific plate [*DeMets and Dixon*, 1999; *Dixon et al.*, 2000]. The Pacific-North America plate boundary runs through the center of the Gulf of California, where it is defined by short spreading segments separated by long transform faults.

[9] Transect 5W runs northwest-southeast from the Los Cabos block, at the southern tip of the Baja California Peninsula, to the East Pacific Rise at the mouth of the Gulf (Figure 1). The Los Cabos block comprises uplifted Mesozoic granitic basement at the southern margin of the peninsula and contrasts with the Miocene volcanic arc strata found east of San Jose del Cabo fault [*Fletcher et al.*, 2000]. These Miocene volcanic arc sequences were formed by eruption of dacitic to andesitic volcanoes and are commonly referred to as the Comondú Group [e.g., *Hausback*, 1984; *Umhoefer et al.*, 2001]. The Comondú Group is mainly

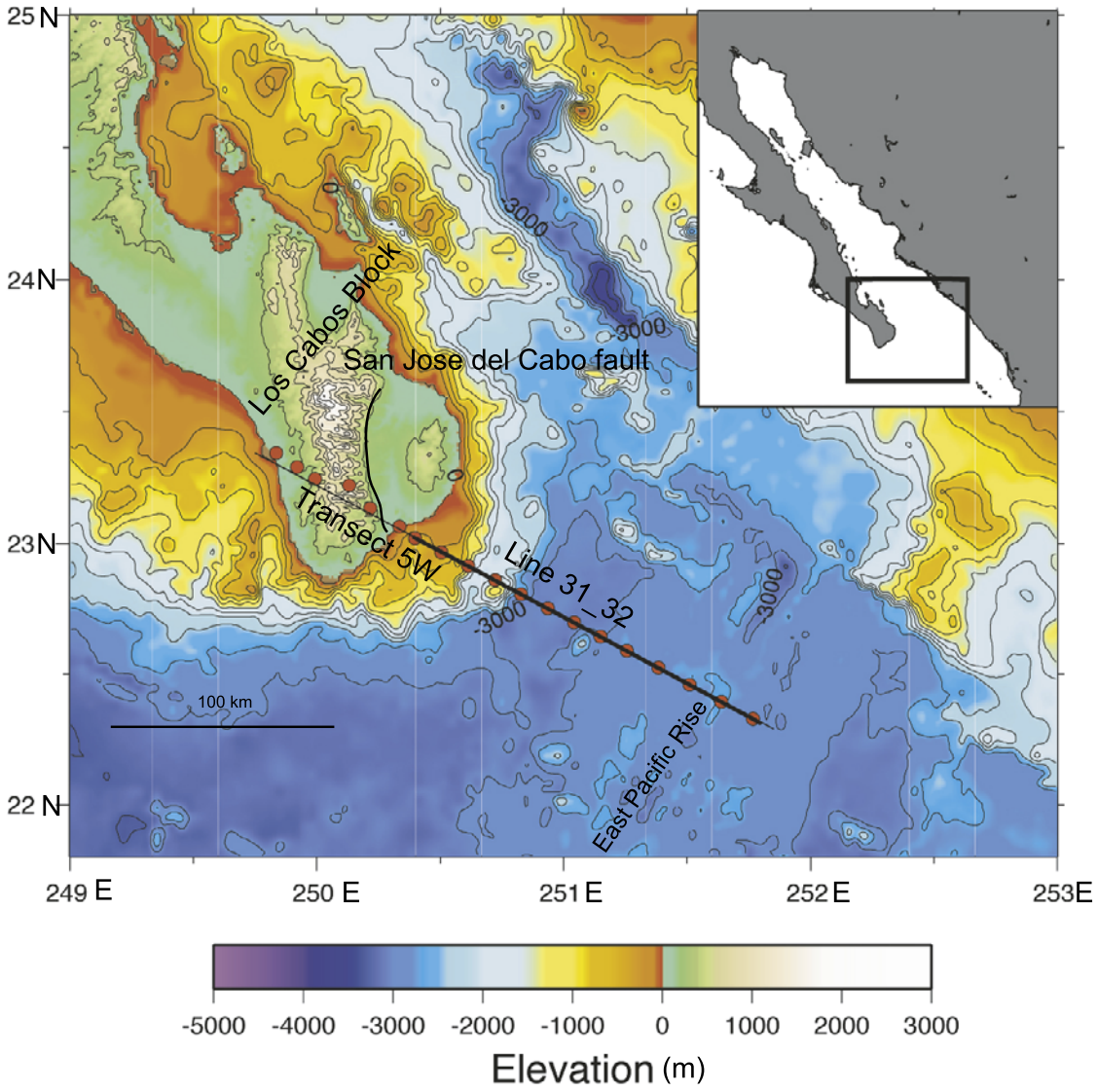

Figure 1. Location of transect 5W displayed on a bathymetric and topographic surface. Transect 5W runs northwest/southeast from the Los Cabos block, at the southern tip of the Gulf of California, to the spreading center in the mouth of the Gulf. The thick black line offshore represents MCS line 31_32. Red circles indicate onshore seismographs and OBS. The thin black line represents the entire length of the velocity model created with the wide-angle data. Onshore the thick black lines represent the location of the San Jose del Cabo Fault.

composed of numerous felsic tuffs, andesite breccia and basalt and andesite lava flows [*Umhoefer et al.*, 2001]. An extensive system of active normal faults is located along the southwestern margin of the GEP [*Fletcher and Munguía*, 2000]. The San José del Cabo fault, which forms part of this system, is an east dipping normal fault with a strike length of ~150 km and a topographic escarpment in excess of 1000 m and forms the eastern limit of the Los Cabos block [*Fletcher et al.*, 2000].

3. MCS Data

[10] Lines 31 and 32 were shot on two different days and were joined to form line 31_32. MCS data from line 31_32 were recorded in the fall of 2002 as part of the PESCADOR experiment with a 480-channel, 6-km-long streamer, aboard R/V *Maurice Ewing*. Shots from the 10 air gun array were fired at constant distance intervals of 100 m. The main steps in the processing sequence of line 31_32 were common midpoint (CMP) sorting, band-pass filtering (20–90 Hz corner frequencies), velocity analysis, normal moveout correction, muting, trim stacking and poststack time migration.

[11] Stacked sections from the MCS reflection data show images of faults and basement structure along line 31_32 (Figure 2). The extended continental crust is dominated by block-faulted basement structure characteristic of nonvolcanic margins [*Chian and Louden*, 1995; *Pérez-Gussinyé et al.*, 2003; *González-Fernández et al.*, 2005].

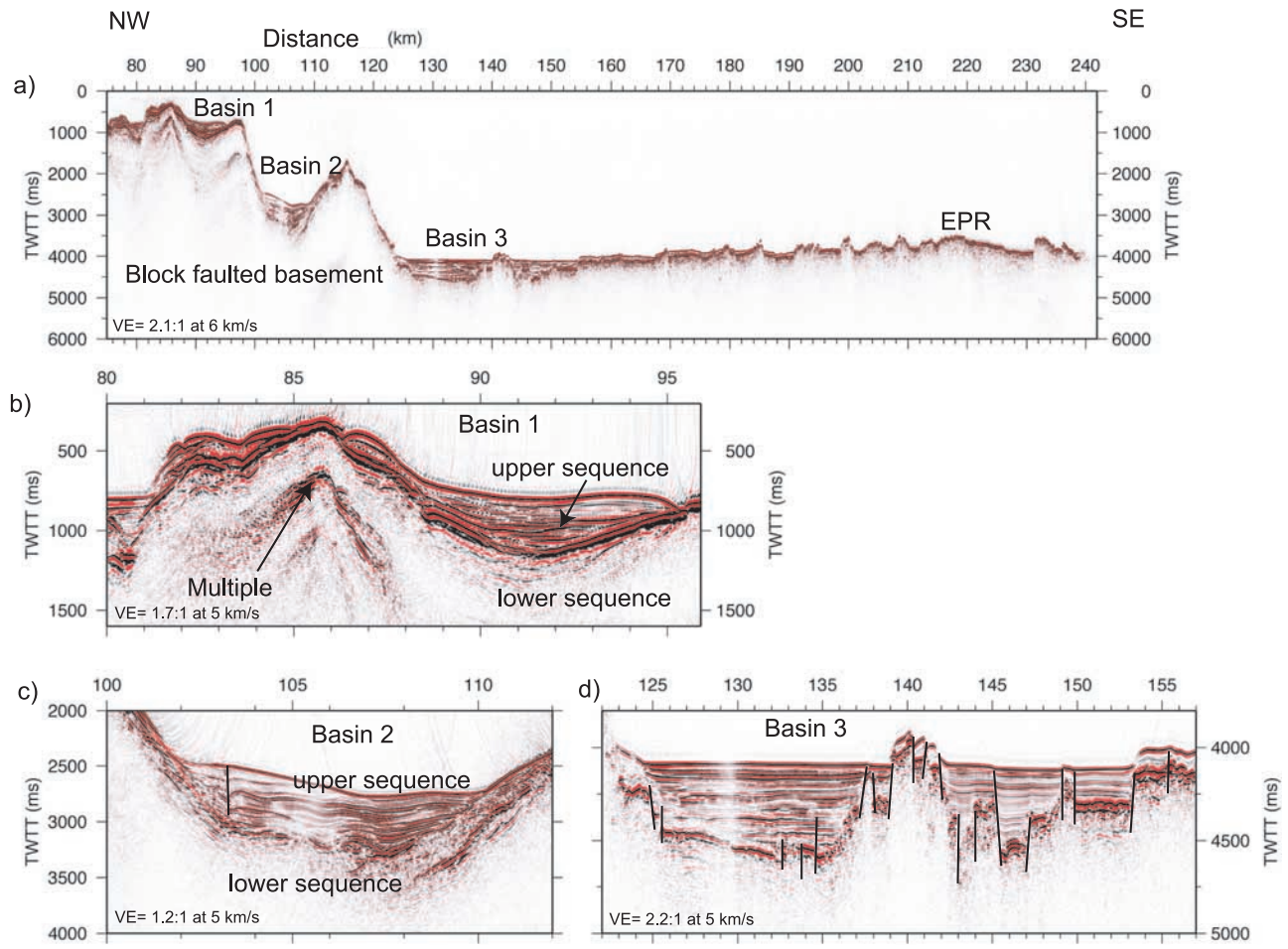

Figure 2. Interpretation of MCS stacked section of line 31_32. (a) Seismic stacked section of line 31_32 indicating the location of the East Pacific Rise (EPR) and basins 1, 2, and 3. Vertical axis is two-way travel time (TWTT) in milliseconds. Horizontal axis is distance in km. Vertical exaggeration of 2.1:1 at 6 km s^{-1} is shown in lower left corner. (b), (c) and (d) Close-ups of the individual basins seen in line 31_32. Solid black lines represent interpreted faults. Vertical exaggeration is indicated at the lower left corner of each panel.

[12] Discrete basins bounded by east dipping normal faults are found on the extended continental crust. Basin-filling sediments are deposited on basement blocks that have been tilted toward the west. The thicknesses of these deposits reach approximately 600 m at model km ~108.

[13] The sedimentary infill of basin 3 is located between model km 125–155 and is deposited on oceanic crust, with the deposit thinning gradually toward the East Pacific Rise. The sediment infill is underlain by a strong reflector interpreted as the top of oceanic basement. This basin is characterized by small basement-cored fault blocks that appear to form Holocene fault scarps on the seafloor (Figure 2d). The area below the strong basement reflector is characterized by a series of broken up reflections of ~500–750 m thickness. This reflectance character is typical of oceanic type basement and is observed in oceanic crust along line 31_32 and in the Alarcon basin [*Sutherland et al.*, 2004]. Basins 1 and 2 are situated between model km 86–95 and 102–110, respectively (Figure 2), and are filled by an upper sequence that lies on a major unconformity above a lower sequence. The lower sequence is highly tilted, indicating that it was deposited before block rotation and is characterized by a series of continuous reflectors of smaller reflection amplitude. Miocene volcanic arc facies of the Comondú Group consist mainly of volcanic breccia and interbedded sandstone and tuffs near La Paz [*Hausback*, 1984] and lava flows and massive breccia near Loreto [*Umhoefer et al.*, 2001] (approximately 100 km and 250 km north of the transect, respectively) and are consistent with the reflectance characteristics of this lower sequence. The upper sequence in basin 2 is characterized mainly by syndepositional deformation; however, this section has a prominent anticline at model km ~103 (Figure 2c) that dies out upward in the uppermost part of the upper sequence. The northwest side of this fold is likely a fault with tilted and less coherent reflectors on the northwest side of the fault. The uppermost section thickens toward the northwest into this feature, supporting its interpretation as a normal fault. The anticline along the interpreted normal fault could have occurred as a consequence of basement block rotation if the normal fault instead is a more complex oblique slip fault. The upper sequence in basin 1 has a

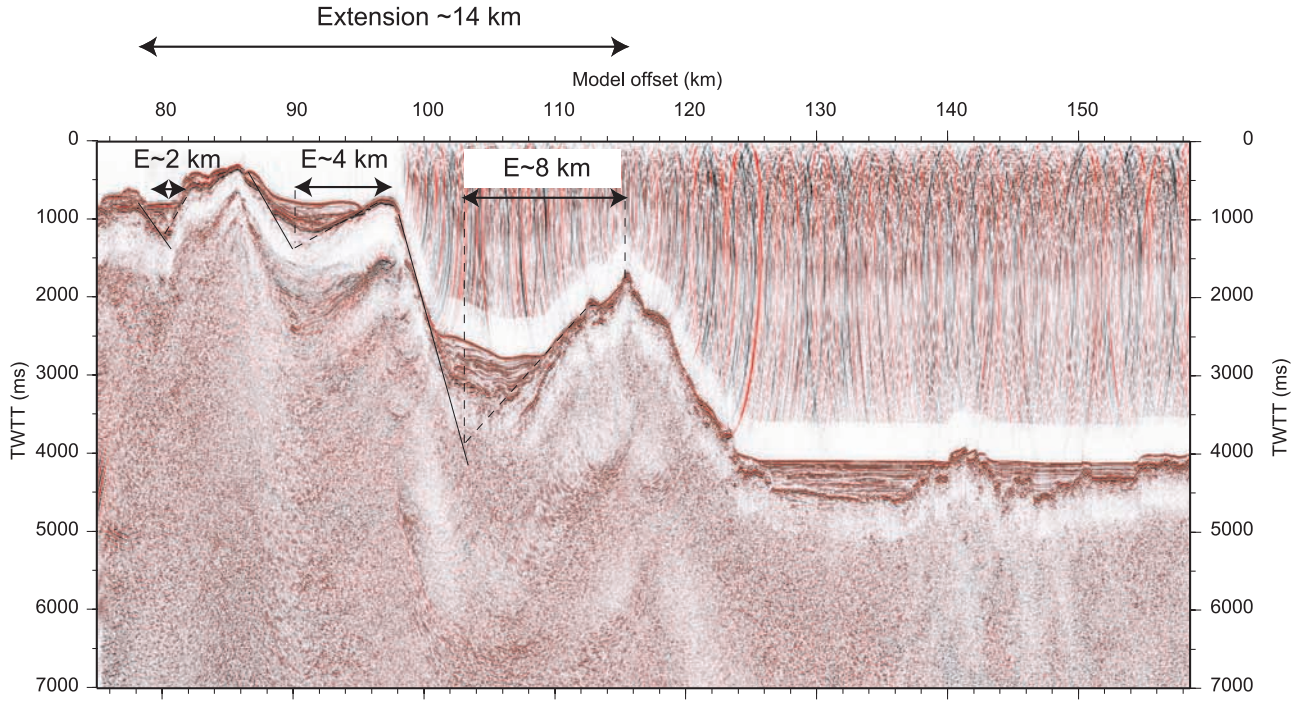

Figure 3. Seismic stacked section of line 31_32 with automatic gain control. Vertical axis is two-way travel time (TWTT) in milliseconds. Horizontal axis is distance in km. Black lines represent the interpreted fault planes. The amount of extension estimated from each fault block is also annotated.

thickness of approximately 400 m with different sets of onlap structures found on the eastern and western margins. This may suggest a complex and episodic depositional history with multiple directions of progradation. However, much of the apparent complexity may also be due to sediment transport out of the plane of the seismic section.

[14] Automatic gain control (AGC) was applied to the seismic stacked section to analyze the reflectivity characteristics of the deeper parts of basement (Figure 3). Other than multiple energy, no coherent reflectivity was observed in the basement. Extension in the upper crust between model km 78 and km 115 was derived from offsets on basement faults imaged on the stacked seismic section. Fault planes were not imaged below the base of the sedimentary basins, and the faults were assumed to be planar for calculating extension. Extension estimates are not significantly altered if this assumption is invalid when the fault angle changes little over the measured vertical offset. Extension of the upper crust between model km 78 and km 115 was estimated to be ~14 km. The amount of extension estimated from the fault heaves is lower than estimates of extension from crustal thickness inferred from the wide-angle data as indicated in section 6.2.

4. Wide-Angle Data

[15] The wide-angle data were recorded by 13 ocean bottom seismometers (OBS) deployed by the R/V *New Horizon* and 6 Reftek seismometers located along the onshore extension of line 31_32. The average spacing for the OBS and Refteks is ~12 km. Shots were fired from the R/V *Maurice Ewing* at 100 m intervals across the entire line; however, a data gap exists over ~40 km near the location of OBS12 and OBS13 due to an error in OBS recording windows. The wide-angle data processing flow involved OBS relocation and digital processing, including minimum phase band-pass (4–15 Hz) filtering and predictive deconvolution (filter window length 0.4 s, 1% prewhitening and predictive distance of 0.05 s) using SIOSeis software.

[16] The nomenclature that we adopt for the seismic phases of the different crustal layers is as follows: upper crust refraction (*Puc*), reflection from the top of lower crust (*PlcP*), lower crust refraction (*Plc*), Moho reflection (*PmP*), and upper mantle refraction (*Pn*). Contrasting patterns of reflections and refractions are observed from continental to oceanic crust. On the oceanic crust a simple pattern is observed, consisting of an upper crust refraction, lower crust refraction, Moho reflection and in some cases upper mantle refraction. This pattern is illustrated in Figure 4a by the record section from OBS7. On record sections from the transitional and continental crust a pattern consisting of upper crust refraction, top of lower crust reflection, Moho reflection and upper mantle refraction is observed. Figure 4b illustrates this pattern on instrument REF4. The pattern change, from instrument to instrument, along the continent-ocean transition can be observed in record sections (see the auxiliary material[1]). Little variation in typical phases or reflection triplications is seen on the oceanic record sections from one instrument to another, indicating no major lateral changes in velocities or crustal boundaries within the oceanic crust. However, on the transitional crust, arrival times from phases vary

[1]Auxiliary material are available in the HTML. doi:10.1029/2007JB005113.

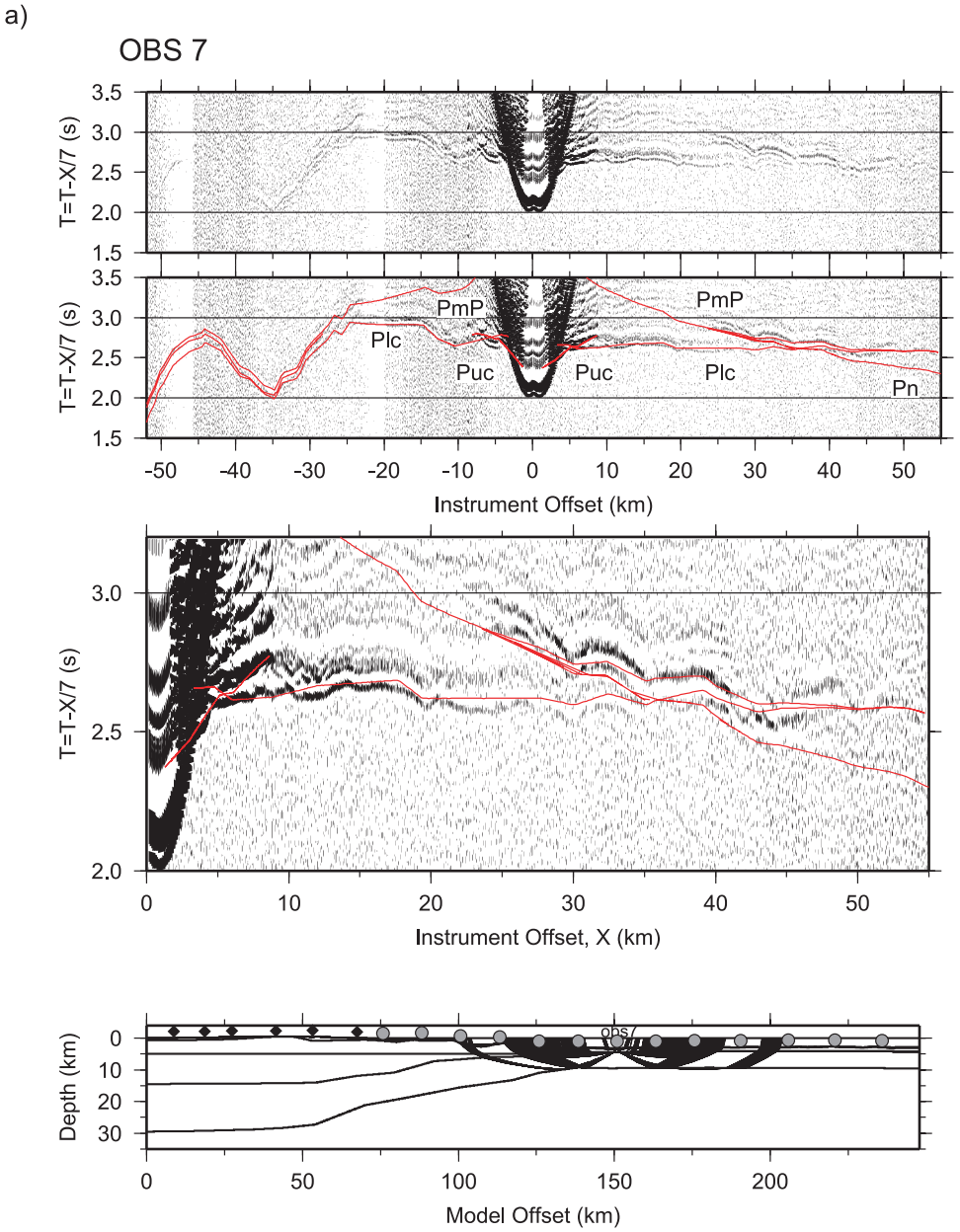

Figure 4a. Top to bottom, plots of processed record section with reduction velocity of 7 km s^{-1} for OBS7, same processed record section overlaid by calculated travel time arrivals (in red), close-up of previous plot corresponding to the travel time arrivals from different phases within the oceanic crust, and ray tracing for the different phases. Black diamonds and gray circles represent the location of the onshore Reftek and offshore OBS, respectively.

considerably with offset, indicating large lateral changes in velocity and/or crustal thicknesses.

5. Velocity Modeling

[17] Traveltime inversion of observed phases produced the final velocity model shown in Figure 5a. Constraints on the velocity and depth of the different interfaces come from reflections from the top of lower crust and Moho and refractions from the upper crust, lower crust and upper mantle. Figure 5b shows the velocity model overlain by the predicted traveltimes, which were two-point ray traced to the offsets of picked (observed) traveltimes. White dots in Figure 5b represent bottoming points of reflected or diving rays. Velocities and crustal thicknesses are well constrained between model km 60–200, where ray coverage and bottoming points are most dense. In the thinned continental crust, the depth of the top of lower crust is well constrained by traveltimes of reflections from this interface seen on Refteks 5, 4, and 3 and OBS1, OBS2, and OBS3. Moho structure and upper mantle velocities are well constrained across the entire continent-ocean transition by 16 instruments recording clear Moho reflections and 10 instruments recording upper mantle refractions.

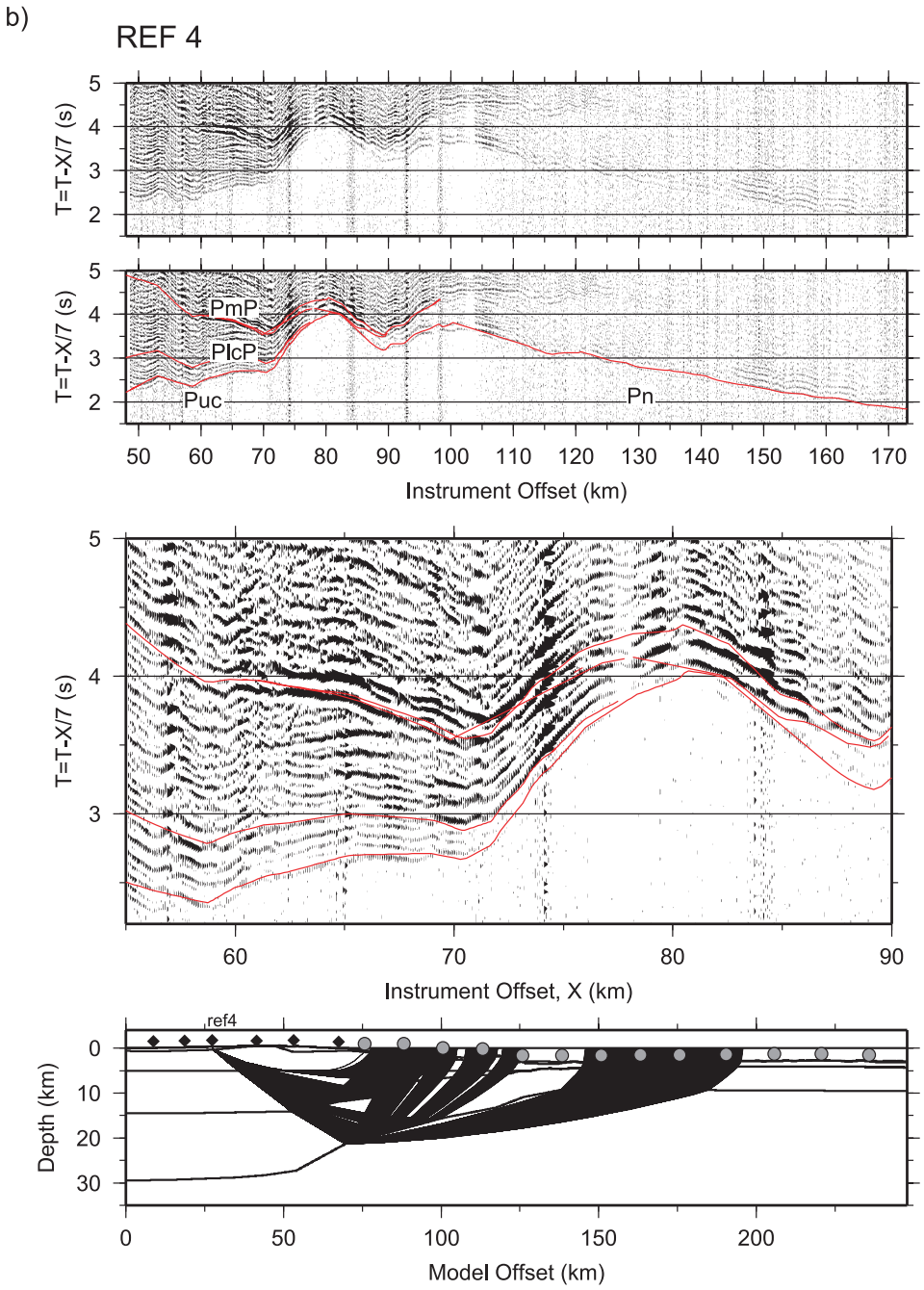

Figure 4b. Top to bottom plots of processed record section with reduction velocity of 7 km s^{-1} for REF4, same processed record section overlaid by calculated travel time arrivals (in red), close-up of previous plot corresponding to the travel time arrivals from different phases within the oceanic crust, and ray tracing for the different phases. Black diamonds and gray circles represent the location of the onshore Reftek and offshore OBS, respectively.

5.1. Methods

[18] We used an iterative inversion method [*Zelt and Smith*, 1992] in order to obtain a crustal-scale velocity model from the wide-angle reflection and refraction data. This technique inverts traveltimes simultaneously to obtain a 2-D velocity and interface structure and requires an initial velocity model and the list of traveltimes and offsets for all different phases.

[19] The initial velocity model used here for the inversion consisted of user-specified velocity values and boundary nodes forming six different layers. The velocity nodes were located at the top and bottom of each boundary and the velocity values were linearly interpolated between nodes. The velocity values and depth of the boundaries were then adjusted through inversion at each node. The stopping criterion for choosing the final model was to minimize the root-mean-square (RMS) traveltime residuals and the χ^2

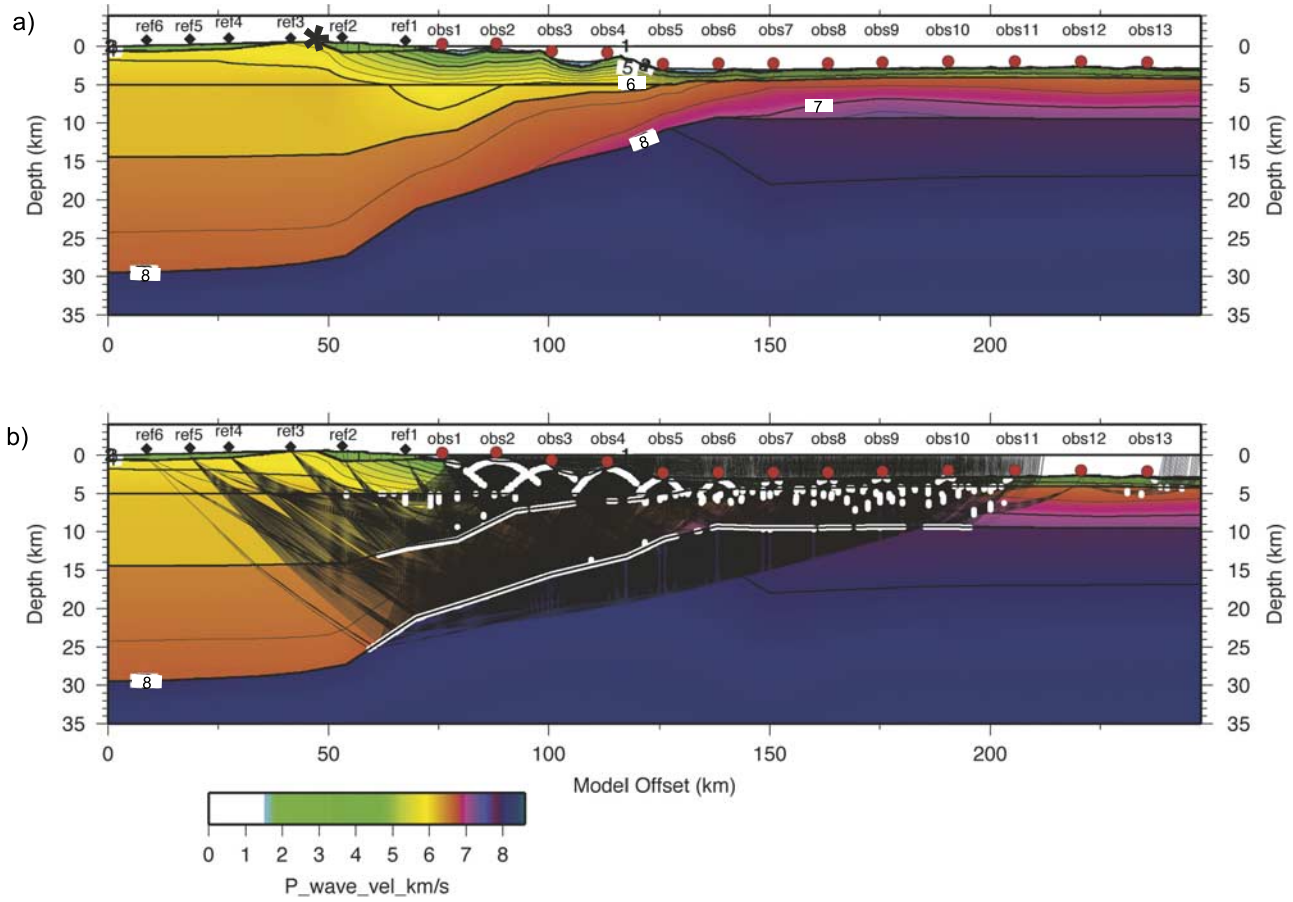

Figure 5. (a) Velocity model from wide-angle data for transect 5W. Black diamonds and red circles represent the position of the Refteks and OBS, respectively. Six Refteks and 13 OBS were used in the model. In general, green (4–5.5 km s^{-1}) in the oceanic crust is indicative of porous basalt, sediment plus basalt, and fractured granite in the continental crust; yellow (6 km s^{-1}) is granite; orange (6.85 km s^{-1}) gabbro; magenta (7+ km s^{-1}) mafic gabbro. The surface location of the San José del Cabo fault is indicated by a gray star between REF3 and REF2. (b) Velocity model overlaid by two-point ray tracing to observed travel time picks. Solid black lines show individual rays and white circles represent bottoming points of all reflected or diving rays.

misfit while tracing the maximum number of rays possible in the model.

5.2. Modeling Steps

[20] The number of layers in the initial velocity model was assigned according to the number of different phases identified in the record sections. The initial velocity model included six layers: (1) water column, (2) sediment cover, (3) basement gradient layer, (4) upper crust, (5) lower crust, and (6) upper mantle. Surface topography and bathymetry values extracted from the shipboard Hydrosweep data form the base of layer 1. MCS stacked images of line 31_32 were used to constrain the basement topography, or base of layer 2. The initial thicknesses of the deeper layers were estimated assuming isostatic equilibrium using typical crustal and mantle densities. Velocity nodes were positioned at a lateral spacing of ~25 km for the upper and lower crust layers to generate stable inversion results. Picked arrival times of the different phases were used for the inversion, and estimates of the pick uncertainties were used for data fitting and weighting during traveltime inversion. The picking of traveltimes of individual phases was done in PLOTSEC software package, and an automated method based on signal to noise ratio was used for assigning pick uncertainties [*Amor*, 1996]. Pick uncertainties typically vary between 25 and 75 ms for upper and lower crustal refractions at near offsets, and are significantly higher for Moho reflections and upper mantle refractions at far offsets (50–150 ms). Traveltimes were inverted simultaneously for velocity and depth nodes until RMS traveltime residuals and the χ^2 misfit were minimized. Table 1 shows the number of data points used in the inversions, RMS traveltime residuals, and χ^2 misfit for each individual phase for each instrument. A total of 12,904 two-point rays were traced with RMS traveltime residuals ranging from 52 to 82 ms among all the different phases.

5.3. Uncertainty Analysis

[21] Estimates of uncertainties in the velocity model were obtained through statistical analysis of key model parameters. We calculated uncertainties of the average depth of the

Table 1. RMS and χ^2 Misfits for All Individual Phases Used for Inversions From Each of the Instruments[a]

Instrument	Parameter	P_{uc}	$P_{lc}P$	P_{lc}	P_mP	P_n	All Phases
All	Number of points	2719	831	2907	3889	2562	
	RMS, ms	0.062	0.082	0.052	0.081	0.075	
	χ^2 misfit	1.358	0.64	1.407	0.955	0.602	
Ref6	Number of points	285	x	x	80	214	579
	RMS, ms	0.072	x	x	0.078	0.099	0.084
	χ^2 misfit	1.597	x	x	1.997	0.73	1.327
Ref5	Number of points	174	78	x	464	482	1198
	RMS, ms	0.043	0.023	x	0.08	0.057	0.064
	χ^2 misfit	0.736	0.272	x	0.935	0.822	0.816
Ref4	Number of points	264	211	x	342	500	1317
	RMS, ms	0.05	0.039	x	0.062	0.064	0.058
	χ^2 misfit	0.929	0.323	x	0.792	0.605	0.672
Ref3	Number of points	264	203	x	422	568	1457
	RMS, ms	0.059	0.097	x	0.108	0.095	0.094
	χ^2 misfit	2.454	0.773	x	2.117	0.721	1.443
Ref2	Number of points	196	x	x	357	500	1053
	RMS, ms	0.059	x	x	0.113	0.069	0.085
	χ^2 misfit	1.795	x	x	2.827	0.358	1.459
Ref1	Number of points	347	x	x	298	x	645
	RMS, ms	0.083	x	x	0.099	x	0.091
	χ^2 misfit	1.512	x	x	0.981	x	1.265
OBS1	Number of points	124	162	x	159	x	445
	RMS, ms	0.06	0.103	x	0.98	x	0.091
	χ^2 misfit	1.055	0.916	x	0.922	x	0.953
OBS2	Number of points	237	92	x	186	x	515
	RMS, ms	0.049	0.061	x	0.56	x	0.054
	χ^2 misfit	0.972	0.32	x	0.369	x	0.636
OBS3	Number of points	197	72	x	85	x	354
	RMS, ms	0.051	0.093	x	0.069	x	0.066
	χ^2 misfit	0.653	0.947	x	0.217	x	0.605
OBS4	Number of points	215	x	x	x	x	215
	RMS, ms	0.038	x	x	x	x	0.038
	χ^2 misfit	0.76	x	x	x	x	0.76
OBS5	Number of points	135	x	220	316	50	721
	RMS, ms	0.038	x	0.054	0.069	0.115	0.064
	χ^2 misfit	0.814	x	1.242	0.326	0.635	0.715
OBS6	Number of points	63	x	448	318	118	947
	RMS, ms	0.015	x	0.057	0.073	0.02	0.058
	χ^2 misfit	0.198	x	1.644	0.247	0.148	0.891
OBS7	Number of points	24	x	485	269	65	843
	RMS, ms	0.011	x	0.049	0.055	0.069	0.052
	χ^2 misfit	0.146	x	0.792	0.261	0.667	0.584
OBS8	Number of points	33	x	490	145	34	702
	RMS, ms	0.012	x	0.045	0.029	0.053	0.042
	χ^2 misfit	0.206	x	1.367	0.328	0.185	1.039
OBS9	Number of points	30	x	348	100	x	478
	RMS, ms	0.014	x	0.047	0.047	x	0.046
	χ^2 misfit	0.208	x	1.503	0.114	x	1.129
OBS10	Number of points	46	x	453	190	106	795
	RMS, ms	0.021	x	0.045	0.039	0.033	0.041
	χ^2 misfit	0.455	x	1.242	0.194	0.105	0.793
OBS11	Number of points	17	x	281	154	x	452
	RMS, ms	0.034	x	0.072	0.075	x	0.072
	χ^2 misfit	0.39	x	2.723	0.581	x	1.902
OBS12	Number of points	x	x	141	x	x	141
	RMS, ms	x	x	0.057	x	x	0.057
	χ^2 misfit	x	x	1.065	x	x	1.065
OBS13	Number of points	8	x	41	x	x	49
	RMS, ms	0.015	x	0.033	x	x	0.031
	χ^2 misfit	0.302	x	0.925	x	x	0.815

[a]Number of points represents the number of data points used in the inversions, RMS is the root-mean-square traveltime residuals. A cross in a column indicates that no phase was picked or used for inversion. Phase P_{uc} corresponds to refractions from the gradient layer and upper crust, phase $P_{lc}P$ corresponds to reflections from top of lower crust, phase P_{lc} is the lower crust refraction, phase P_mP is Moho reflection, and P_n is upper mantle refraction.

top of lower crust and Moho in the transitional crust between nodes situated at model km 85 and 125. A perturbation of depth nodes from the final model was applied independently to the top of lower crust and Moho. Traveltime residuals and the χ^2 misfit were minimized after each perturbation by inverting for interface depth while maintaining the velocity gradient above the boundary. Depth uncertainties were later estimated using the F test [*Zelt and Smith*, 1992]; the maximum perturbation that allowed a comparable fit to the observed data at the 95% confident level was used as an estimate of the depth uncertainty. This method produces estimates of the average

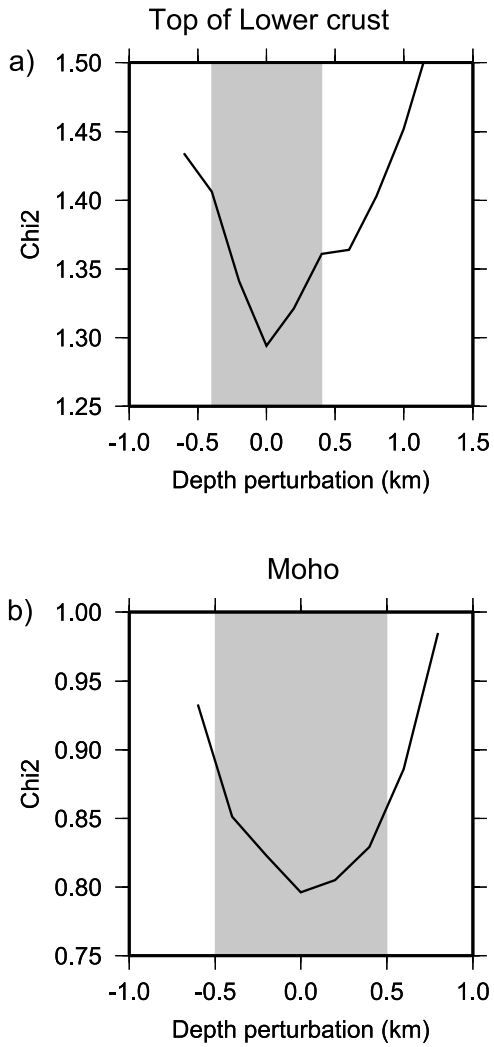

Figure 6. The χ^2 versus depth perturbation for (a) the top of lower crust and (b) Moho between nodes situated at model km 85 and 125. The shaded area represents the depth uncertainty of each layer calculated using the F test. Models created by a depth perturbation of less than gray shaded area are considered statistically similar models.

depth uncertainty of the top of lower crust and Moho and not estimates of the lateral variations of depth uncertainties. However, the depth variations along these boundaries were already well resolved by the fit of the slopes of the refracted and reflected phases of the layers above the boundary. This procedure has been previously used to calculate the uncertainty in the average depth of a boundary in continental rifted studies from wide-angle seismic data [*Dean et al.*, 2000; *Pérez-Gussinyé et al.*, 2003]. Figure 6 shows the minimized χ^2 misfit versus depth perturbation for each of these boundaries. Depth perturbations that fall within the shaded area on Figure 6 produce statistically identical models at the 95% confident level. Uncertainties of ±0.4 km were estimated for the average depth of the top of lower crust and Moho.

5.4. Gravity Modeling

[22] Gravity modeling (Figure 7) is used for estimations of crustal densities to add constraints to the velocity model where poor ray coverage does not allow crustal structure to be determined. It also constitutes an important check on the seismic velocity model in places where high ray coverage exists. Here a direct conversion of the velocity model to a crustal density model was made using a composite function as described by *Lizarralde and Holbrook* [1997]. Since densities in the upper mantle of young lithosphere are a function of distance to the ridge axis, the densities below the Moho were temperature-corrected with a finite difference solution to the one-dimensional (1-D) heat equation. Gravity anomalies from the density model were then calculated by 2-D gravity modeling using a wave number domain algorithm similar to that described by *Blakely* [1996].

[23] Offshore, the gravity anomalies calculated from the model were compared to observed free-air gravity anomalies from the R/V *Maurice Ewing* gravimeter. Onshore, the velocity model was truncated above sea level and the calculated gravity anomalies were compared to Bouguer gravity anomalies derived from a gridded data set of terrain-corrected, free-air gravity anomaly measurements [*National Geophysical Data Center*, 1999].

[24] Offshore, in places where ray coverage was high in the velocity model, the calculated and observed gravities matched well (±5 mGal). In places with low ray coverage, the densities were later adjusted to minimize mismatch between observed and calculated gravity anomalies. Mainly this adjustment was done on densities of the lower oceanic crust between model km 190 and 230, where the model was poorly constrained due to a gap in ray coverage. Since this area lies on the East Pacific Rise where melt is expected in the crust, the densities in this area were slightly reduced from those originally obtained from the direct conversion from velocities to densities.

[25] Gravity anomalies calculated from the adjusted density model closely fit the observed anomaly over the continent-ocean transition and oceanic crust (Figure 7a). The distinct free-air gravity highs observed at model km ~95 and ~120 are explained by the existence of higher densities at shallow depth and correspond to basement highs of the tilted basement fault blocks. The free-air gravity lows observed in the continent-ocean transition correspond to the location of the sedimentary basins. Onshore, ray coverage is lacking in the deepest layers between model km 0–40 (Figure 5b). The continental crust was thinned at these offsets to minimize the mismatch between observed and calculated gravity values. The combination of the seismic and gravity modeling constrains the crustal thinning across the continent-ocean transition.

6. Results and Discussion

[26] The final velocity model indicates distinct changes in crustal structure from continental to oceanic crust. The crust thins from ~28 km in continental crust to ~6.7 km in oceanic crust, and the thinned continental crust occupies a ~75-km-wide zone.

6.1. Oceanic Crust, Mantle Upwelling Ratio, and Temperature

[27] The upper oceanic crust, or layer 2, is formed by a ~1.5-km-thick layer with velocities indicative of basalt and porous basalt (4.3–5.5 km s^{-1}). The lower oceanic crust, or

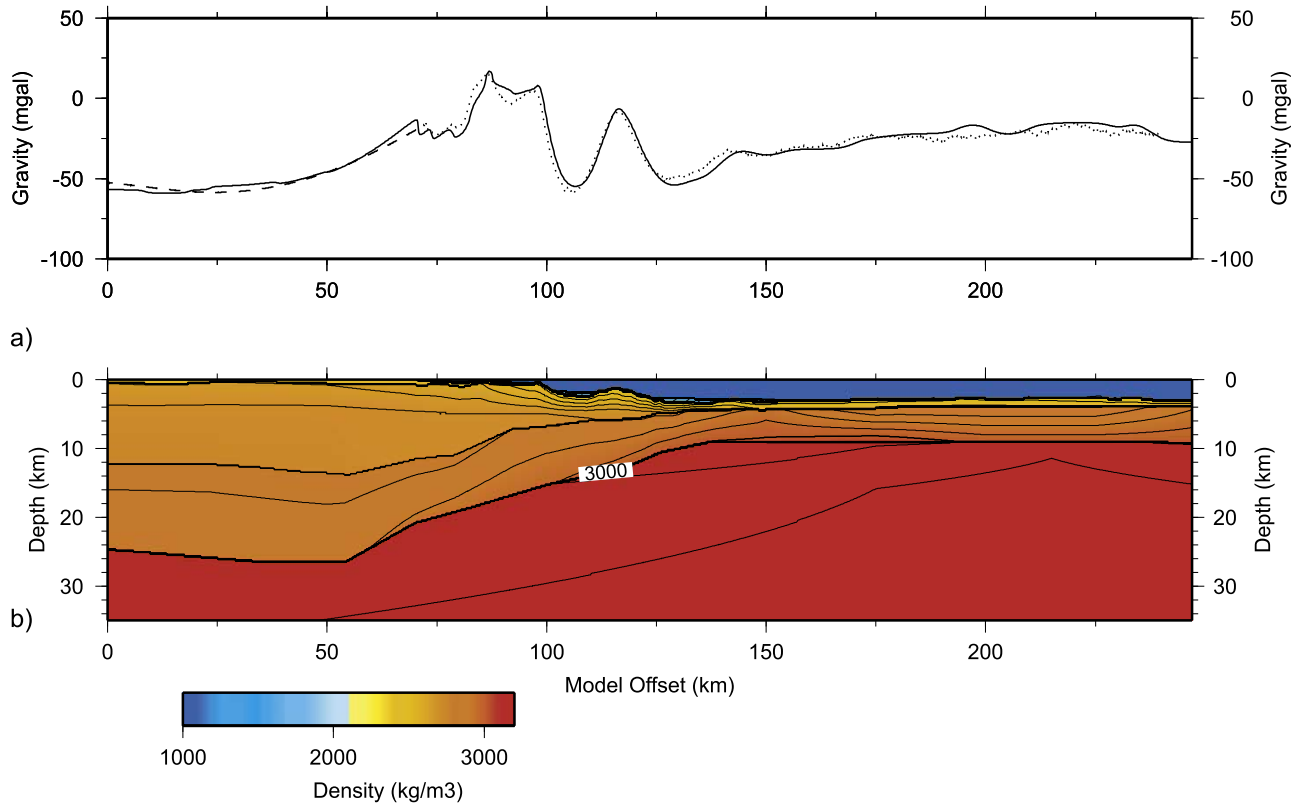

Figure 7. (a) Free-air and Bouguer gravity anomaly profiles along transect 5W. Offshore, dotted line represents the free-air gravity anomalies from the R/V *Maurice Ewing* gravimeter. Dashed line onshore corresponds to the Bouguer gravity anomaly profile derived from a gridded data set of terrain-corrected, free-air gravity anomaly measurements [*National Geophysical Data Center*, 1999]. Solid line represents the gravity anomaly profile calculated from the density model. (b) Adjusted density model calculated from the velocity model.

layer 3, is formed by a ~5.2-km-thick layer with velocities indicative of gabbro and mafic gabbro (6.5–7+ km s^{-1}). No seismic reflections have been identified from the layer 2/3 boundary in the seismic records. This suggests a transition zone from the upper, altered and porous, layer and the lower, unaltered, layer rather than a first-order discontinuity between two lithologically different layers [*Detrick et al.*, 1994]. One-dimensional velocity profiles at the locations of OBS7, OBS8, OBS9 and OBS10, extracted from the 2-D velocity model, are shown in Figure 8. These locations are on oceanic crust where there is good ray coverage and velocities and depth of crustal boundaries are well constrained. OBS7 and OBS8 show slightly lower average velocities and slightly lower crustal thickness than OBS9 and OBS10. In general, little lateral variation in crustal thicknesses and velocities is observed in the oceanic crust. This suggests a fairly constant rate of magmatic productivity, assuming that the spreading rate has been constant in this area since ocean floor spreading began approximately 3.6 Ma [*DeMets*, 1995].

[28] Crust of a certain thickness produced by passive or active mantle upwelling differ in major element composition due to differences in the pressure and fraction of melting achieved during both mechanisms [*Klein and Langmuir*, 1987]. Crustal thickness and MgO content both increase with increasing mantle potential temperature for crust made purely through the efficient extraction of melts generated by passively upwelling mantle [*Klein and Langmuir*, 1987]. To make the same thickness crust at a lower mantle temperature, active mantle upwelling is needed, which produces crust with lower MgO and higher SiO_2 content decreasing mean crustal velocities [*Kelemen and Holbrook*, 1995]. Seismic velocities and crustal thickness can thus be used to estimate mantle thermal conditions and upwelling ratios during rifting [*Kelemen and Holbrook*, 1995; *Canales et al.*, 1998; *Holbrook et al.*, 2001; *Korenaga et al.*, 2002; *Sallares et al.*, 2003; *Sallares and Charvis*, 2003]. However, because of porosity effects in the upper oceanic crust, seismic velocities provide useful petrological information only in the lower oceanic crust [*Korenaga et al.*, 2002]. Calculations of crustal thickness and mean lower crustal velocities from the velocity model are here compared to those predicted by *Holbrook et al.* [2001] to estimate mantle temperature conditions and upwelling ratios. Those predictions are calculated by first obtaining the melt fraction at a given pressure along a decompression melting trend at a given potential temperature using the adiabatic, equilibrium melting model from *McKenzie and Bickle* [1988] and then calculating V_p using equation (2) of *Kelemen and Holbrook* [1995]. Here the observed mean lower crustal velocity for the oceanic crust is calculated from the velocity model and corrected to a temperature of 400°C and confining pressure

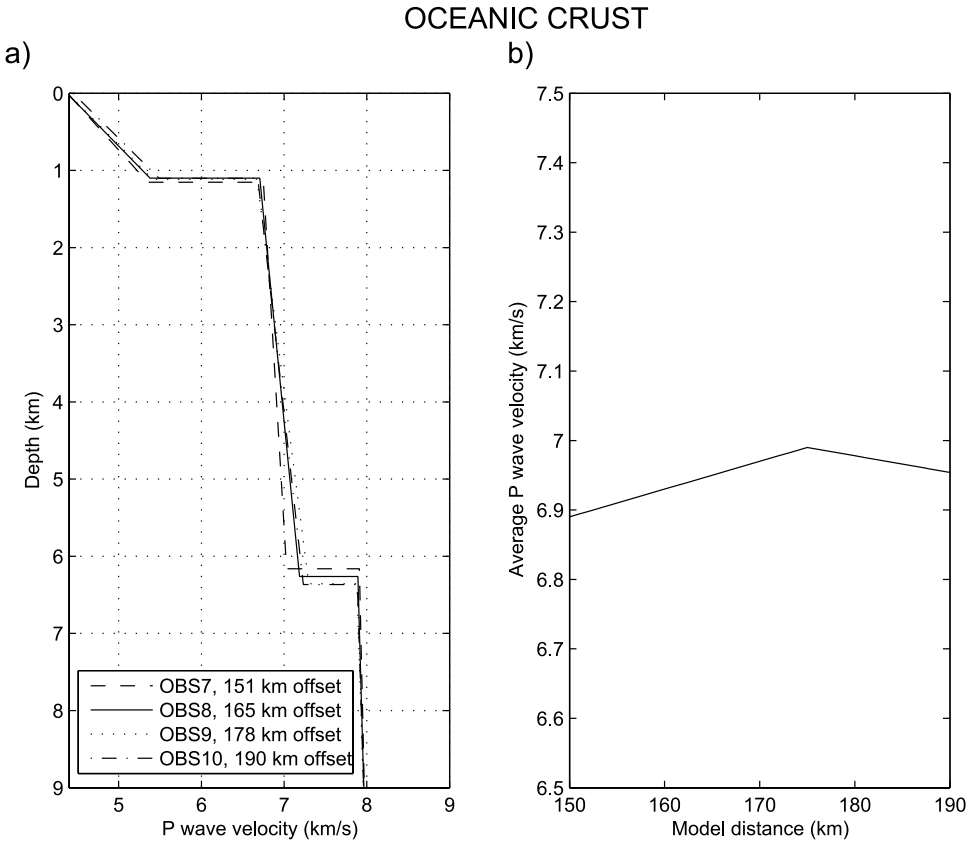

Figure 8. (a) Oceanic crust velocity profiles pulled from the 2-D velocity model, at the locations of OBS7, OBS8, OBS9, and OBS10. (b) Average velocity for the igneous oceanic crust along the location of OBS7, OBS8, OBBS9, and OBS10 calculated from the velocity model.

of 600 MPa by applying pressure and temperature corrections of 0.00022 km s^{-1} MPa^{-1} and −0.0005 km s^{-1} $°C^{-1}$, respectively [*Holbrook et al.*, 2001]. On the basis of the velocity model results, and after applying the pressure and temperature corrections, the average oceanic crust thickness for OBS7, OBS8, OBS9, and OBS10 is ∼6.2–6.3 km, and the average velocity for the oceanic lower crust is ∼6.9–7.0 km s^{-1}. Figure 9 shows these mean crustal velocities and thickness calculated from the velocity model along with the predicted mean crustal velocities vs. crustal thickness for different mantle upwelling ratios (X) and temperatures from Holbrook's predictions. The calculated average lower crustal velocities and thicknesses are in accordance with predictions for passive upwelling mantle and normal mantle temperatures ∼1300°C. The lack of evidence of synrift intrusive or extrusive magmatism in the transitional crust also supports these observations. These observations indicate normal (not enhanced) upper mantle temperatures at the time of initial seafloor spreading.

6.2. Continental Crust, Stretching Factors, and Extension

[29] West of the San Jose del Cabo fault, the upper continental crust is formed by a ∼14-km-thick layer with velocities varying from ∼6 to ∼6.2 km s^{-1}, indicative of granitic rocks (Figure 5). These velocities are consistent with the uplifted Mesozoic granitic basement of the Los Cabos Block situated west of the San Jose del Cabo Fault

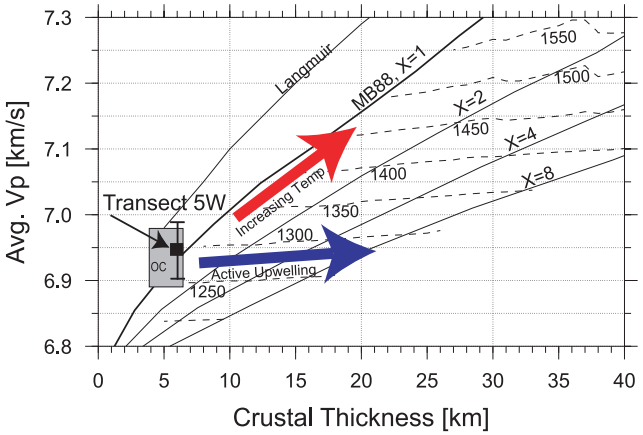

Figure 9. Predicted mean crustal velocity versus crustal thickness for the *Langmuir et al.* [1992] passive upwelling model (thin line) and *McKenzie and Bickle* [1988] model for different upwelling ratios, X (figure from *Holbrook et al.* [2001]). Dashed lines represent mantle potential temperatures for the McKenzie and Bickle model. OC represents the calculated mean crustal velocity and thickness near the East Pacific Rise [*Canales et al.*, 1998]. Large arrows represent the isolated effects of increased temperature, and increased active upwelling. Small black square represents the mean crustal thickness and velocities obtained from the velocity model at instruments OBS7, OBS8, OBS9, and OBS10.

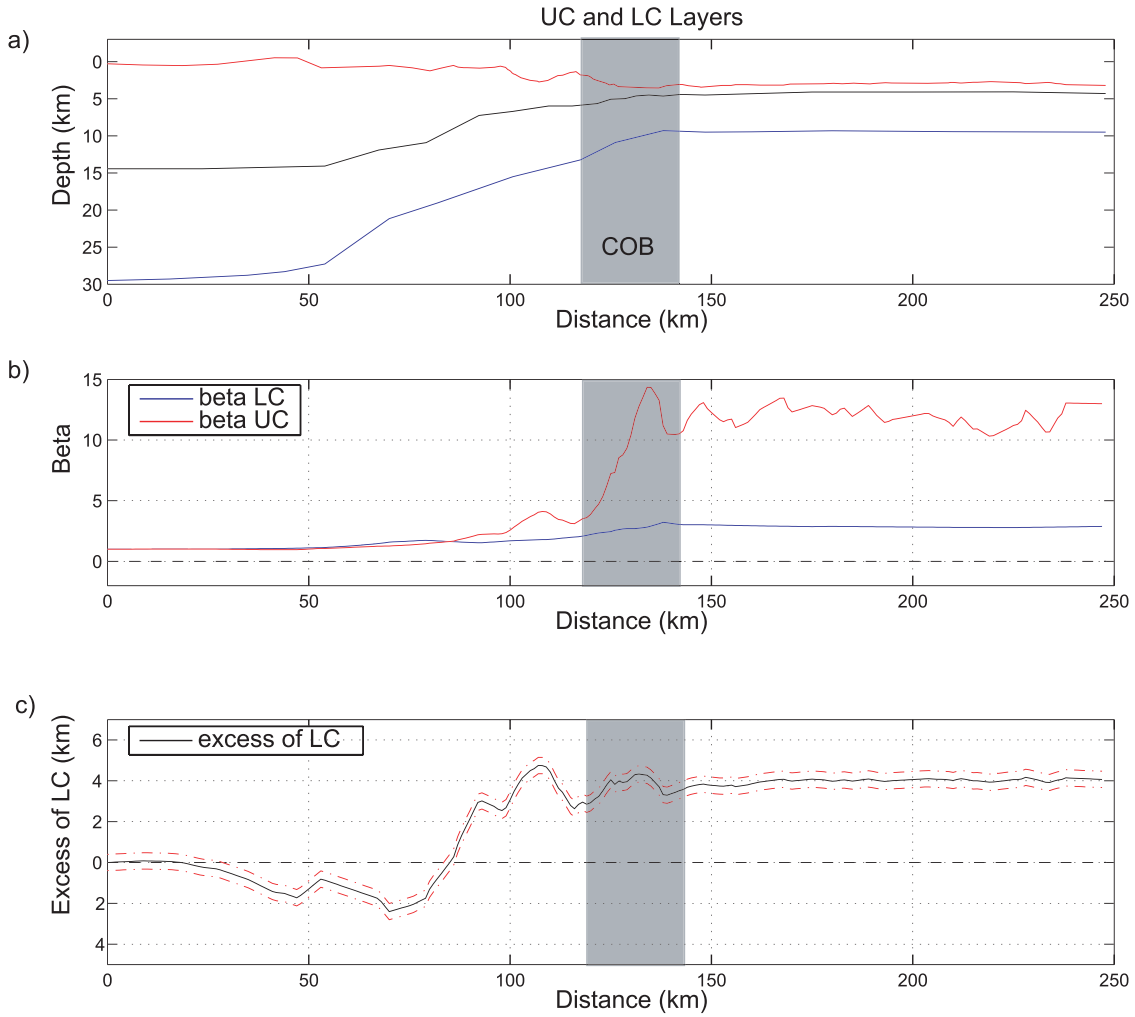

Figure 10. (a) Upper crust and lower crustal boundaries shown on a depth section. Red line represents the top of crystalline basement. Black and blue lines correspond to the top of the lower crust and Moho, respectively. Shaded gray box represents the continent-ocean boundary (COB). (b) Red and blue lines represent the stretching factor for the upper and lower crust, respectively. (c) Black solid line indicates the excess of lower crust between model km 60 and the COB. Red line indicates the uncertainty in excess of lower crust (±0.4 km). Between model km 60 and 85, lower crust is stretched slightly more than the upper crust, and a slight deficit of lower crust is found. Between model km 85 and the COB, the stretching factor for the upper crust increases more rapidly than the stretching factor for the lower crust, and an excess of lower crust is found.

[*Fletcher et al.*, 2000]. Lower basement velocities (~4.0–5.5 km s^{-1}) are found east of the San Jose del Cabo fault. There, crystalline rocks are penetratively fractured [*Fletcher and Munguía*, 2000], and the lateral change in velocity seen at model km ~55 is interpreted as the result of fractured and faulted granite located east of the fault [*Fletcher et al.*, 2003]. Lower crustal velocities in the continental and transitional crust vary from ~6.50 to ~6.75 km s^{-1} and are representative of more mafic composition rocks such as anorthosites (assuming no hydration or fracturing) [*Christensen and Mooney*, 1995]. The thickness of the upper and lower crust varies laterally in the transitional crust from NW to SE, with a total length of extended continental crust of ~75 km.

[30] To understand the deformation of crustal layers, we computed stretching factors for upper and lower crust along the continent-ocean transition, across which the upper crust thins from ~14 km to ~1.5 km and the lower crust thins from ~14 to ~7 km. Figure 10b shows the stretching factor, β, for the upper and lower crust along transect 5W between model km 60 and 135. The difference in stretching magnitude suggests a different extensional behavior for the upper and lower crust. Depth-dependent stretching factors have been observed on several different rifted continental margins, and their analysis is often used to infer the mechanism of extension [*Driscoll and Karner*, 1998; *Pérez-Gussinyé et al.*, 2003]. Similar stretching factors for upper and lower crust would indicate that extension of the upper crust and lower crust took place in a uniform manner [e.g., *McKenzie*, 1978]. On the basis of the stretching factors shown in Figure 10b and calculating the lower crust thickness necessary for β(lower crust) = β(upper crust), an excess of lower crust

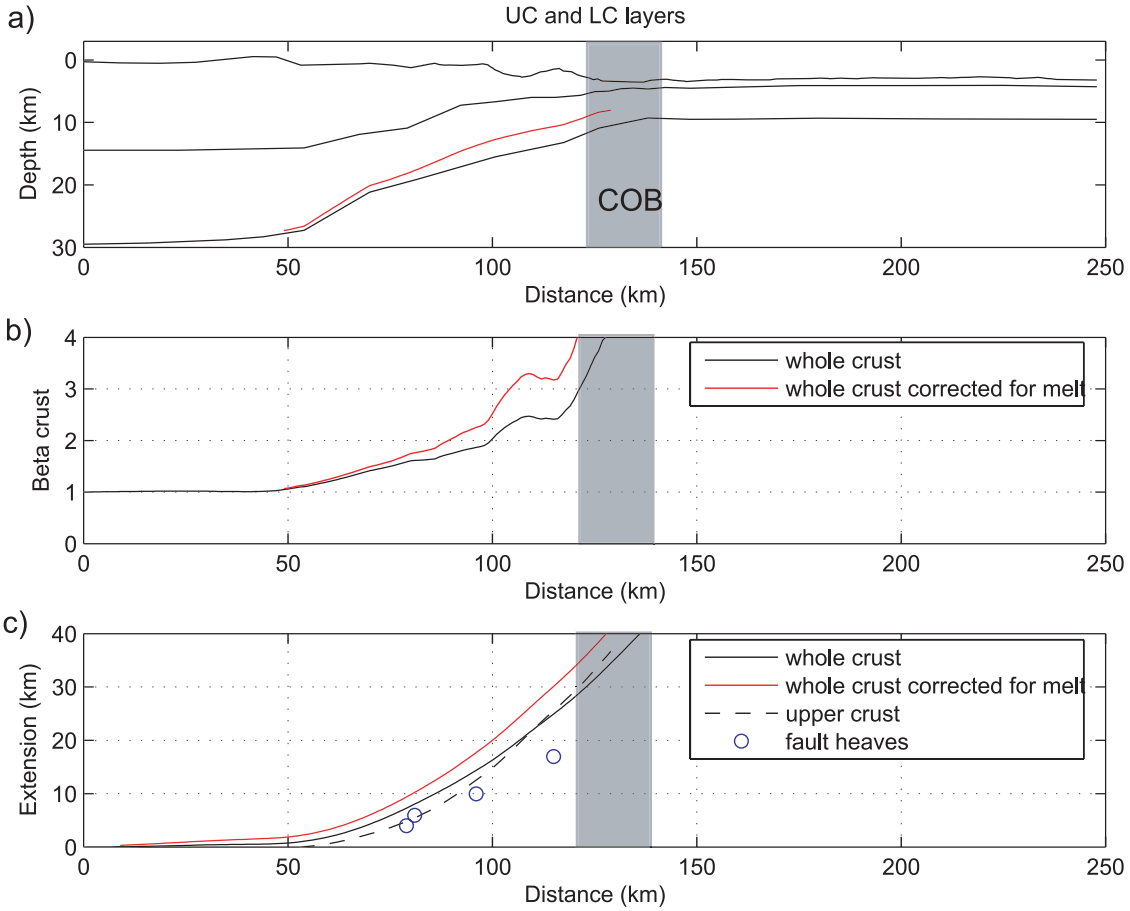

Figure 11. (a) Upper crust and lower crustal boundaries shown on a depth section. Red line indicates the Moho depth corrected for the melt produced by extension of the continental lithosphere. Shaded gray box represents the continent-ocean boundary (COB). (b) Crustal stretching factor, β, for the whole crust calculated from model km 0 to the COB. (c) Amount of total crustal extension calculated by integrating $(1-1/\beta)$ from model km 0 to the COB. Blue circles indicate the amount of extension estimated from the fault heaves.

thickness of up to ~5 km is found between model km ~85 and 125 (Figure 10c). The excess of lower crust found in this area is well resolved, considering the depth uncertainty of ±0.4 km of the top of lower crust and Moho calculated previously at these offsets (Figure 6). A slight deficit of lower crust is also observed between model km ~60 and 85. However, this lower crust deficit is too small to account for the excess of lower crust found between model km 85 and 125. The idea of lower crustal flow in nonvolcanic continental rifted margins in the absence of mantle temperature anomalies has been previously suggested to explain differential thinning of the upper and lower crust [*ter Voorde et al.*, 1998; *Pérez-Gussinyé et al.*, 2003]. Crustal thickness variations produce lateral pressure differences in the crust that might drive flow of the hot and weak portions of the deepest crust [*Buck*, 1991]. The predominately brittle or semibrittle deformation of narrow rift mode might have driven small-scale flow of the deepest crust to account for the local excess of lower crust. However, the excess of lower crust might also be explained by melt produced by extension of the continental lithosphere. A lateral increase from 6.55 to 6.75 km s^{-1} in average lower crustal velocity is observed between model km ~85 and 125 (Figure 5). In order to assess if the lateral increase in average lower crustal velocity could be caused by intruded igneous rocks produced by melting during extension of the continental lithosphere, we estimated the amount of rift-related melt necessary to increase the average lower crustal velocity by 0.2 km s^{-1} and compared it to estimates of melt from *McKenzie and Bickle* [1988]. First we calculated the fraction, F, of present-day lower crust that represents magmatic material of velocity, V_{mag}, intruded during rifting. F can be described as

$$F(x) = \{[1/V_{lc}(x)] - (1/V_{ref})\}/\left[\left(1/V_{mag}\right) - (1/V_{ref})\right]$$

where $V_{lc}(x)$ is the average lower crust velocity at model offset x and V_{ref} is the reference lower crust velocity (6.55 km s^{-1}). F was calculated for V_{mag} = 7.0, which is the average velocity of the lower oceanic crust near the continent-ocean boundary. The thickness of the rift-related magmatic additions was calculated by multiplying F(x) by the present-day lower crustal thickness. Figure 11a shows the thickness of the rift-related melt across model km ~85–125.

The maximum thicknesses are concentrated near the continent-ocean boundary where approximately 3 km of melt would have been generated if material of $V_{mag} = 7.0$ were intruded.

[31] The volume of melt generated by extension of the continental lithosphere depends on the potential temperature of the upper mantle, the thickness of the mechanical boundary layer and the amount of stretching [*McKenzie and Bickle*, 1988]. Stretching factors of ~2 to 4 were here estimated from crustal thickness variations corrected for the intruded melt thickness between model km ~85–125 (Figure 10b). Estimates of lithospheric thickness in this area range from ~100 km [*Clayton et al.*, 2004] in the central parts of the peninsula of Baja California to ~125 km [*Artemieva and Mooney*, 2001] at the southern tip of the peninsula. According to *McKenzie and Bickle* [1988], for potential mantle temperatures of 1280°C, a mechanical boundary layer of ~100–125 km, and a stretching factor of ~4, melt thickness of ~1 km will be generated by extension of the lithosphere. This amount of melt does not account for the total excess of lower crust of up to 5 km observed between model km ~85 and 125 or for the thickness of rift-related melt (3 km) necessary to increase lower crustal velocities by 0.2 km s^{-1}. Therefore the excess of lower crust should be caused by either a large-scale structural asymmetry in the margin or by lower crustal flow. These two hypotheses can be further tested by analyzing the wide-angle data from the conjugate margin, which is being processed independently [*Brown et al.*, 2005].

[32] The crustal thinning profile across the continent-ocean transition is defined by the seismic results and the gravity modeling, providing the basis for estimating the total crustal extension. The crust thins from ~28 km in continental crust at model km ~40 to ~6.7 km in oceanic crust at model km ~125. The total amount of extension was calculated by integrating $(1-1/\beta)$ from model km 0 to the continent-ocean boundary (Figure 11c). Total extension in the direction of transect 5W of the whole crust corrected for the melt intruded is estimated to be ~35 km (Figure 11c). Upper crustal extension of ~30 km was estimated from the crustal thickness variations of the velocity model and ~18 km from the fault heaves (Figure 11c). The amount of upper crustal extension derived from upper crustal faulting is significantly less than that of the whole crust as has been observed in several other rifted margins [*Davis and Kusznir*, 2004; *Reston*, 2007].

6.3. Rift Evolution and Comparison to Other Nonvolcanic Margins

[33] Wide-angle seismic data from transect 5W and Alarcon and Guaymas basins show significant differences in seismic structure along the Gulf of California [*Lizarralde et al.*, 2007]. The northern margin of the Alarcon basin, situated just ~100 km north of transect 5W, has a ~300-km-wide zone of extended continental crust dominated by normal faulting at the surface and an average crustal velocity of 6.2 km s^{-1} [*Sutherland et al.*, 2004]. The oceanic crust found in Alarcon basin is very similar to that seen in transect 5W and has a thickness of ~6.5–7 km with lower crustal velocities of ~6.8 km s^{-1} [*Sutherland et al.*, 2004; *Lizarralde et al.*, 2007]. This may suggest a similar initial mantle temperature and upwelling ratio at the time of breakup as for transect 5W. However, the seismic structure along the Alarcon basin represents a more distributed extension before necking. The Guaymas transect, located ~200 km north of transect 5W, indicates abrupt necking and thick new igneous crust (~8–12 km) [*Lizarralde et al.*, 2003, 2007]. These differences in seismic structure from north to south along the axis of extension in the Gulf of California vary over short lateral distances (<200 km) and have been attributed to variability in mantle fertility, possibly assisted by sedimentary insulation [*Lizarralde et al.*, 2007].

[34] In this study we compare transect 5W with other nonvolcanic margins from the North Atlantic and Greenland-Labrador conjugate pair to gain insight on the influence of key parameters on the rift-to-drift evolution of transect 5W. The abruptness and nature of the continent-ocean transition are mainly controlled by crustal thickness, crustal composition, thermal conditions, strain rate, and mantle rheology [*Buck*, 1991; *Behn et al.*, 2002]. Crustal structure and seismic velocities found between typical continental and typical oceanic crust provide insight into the mechanism of continental rifting and its evolution to seafloor spreading [e.g., *Holbrook et al.*, 1994; *Whitmarsh and Sawyer*, 1996; *Dean et al.*, 2000; *Pérez-Gussinyé and Reston*, 2001; *Shillington et al.*, 2006]. Some similarities and differences are found between the rift architecture of transect 5W and other nonvolcanic rifted margins from the North Atlantic and Labrador-Greenland conjugate margins. A comparison of the seismic structure from transect 5W with these other nonvolcanic margins is shown in Figure 12. The transition between typical continental and typical oceanic crust differs in nature for each one of these transects. The transitions from continental to oceanic crust across the nonvolcanic margins of the North Atlantic and Labrador-Greenland conjugate margins are characterized by a thin upper layer (<3 km thick) with velocities between ~4.0 km s^{-1} at the top and ~6.5 km s^{-1} at the bottom of the layer, and a high-velocity deeper layer (~7.5 km s^{-1}) [e.g., *Pinheiro et al.*, 1992; *Chian and Louden*, 1995; *Chian et al.*, 1995; *Dean et al.*, 2000; *Funck et al.*, 2003].

[35] On the Labrador-Greenland conjugate margins, velocities in this deeper layer range from 6.4 to 7.7 km s^{-1} and are nearly symmetrically distributed between extended continental crust and typical oceanic crust [*Chian and Louden*, 1994, 1995] (Figure 12a). The extended continental crust is wider on the Labrador margin than on the Greenland margin; this asymmetry was attributed to migration of crustal necking produced by enhanced cooling and strengthening of the rift zone [*Chian and Louden*, 1995; *Bassi et al.*, 1993]. Results from the Newfoundland SCREECH1 transect show a ~90-km-wide zone of extended continental crust followed by ~80-km-wide zone of thin crust underlain by serpentinized mantle [*Funck et al.*, 2003] (Figure 12b). The Iberia IAM-9 transect comprises ~60 km of extended continental crust and a ~170-km-wide zone of 2- to 4-km-thick upper crust, with velocities of 4.5–7 km s^{-1}, and up to 4-km-thick deeper layer composed of exposed upper mantle with velocities of ~7.6 km s^{-1} [*Dean et al.*, 2000] (Figure 12c). The relatively small volume of melt and the higher velocities found in the deeper layer of these four margins were explained by slow spreading rates (<20 mm a^{-1}) and partial serpentinization of mantle peridotite. Transect 5W is

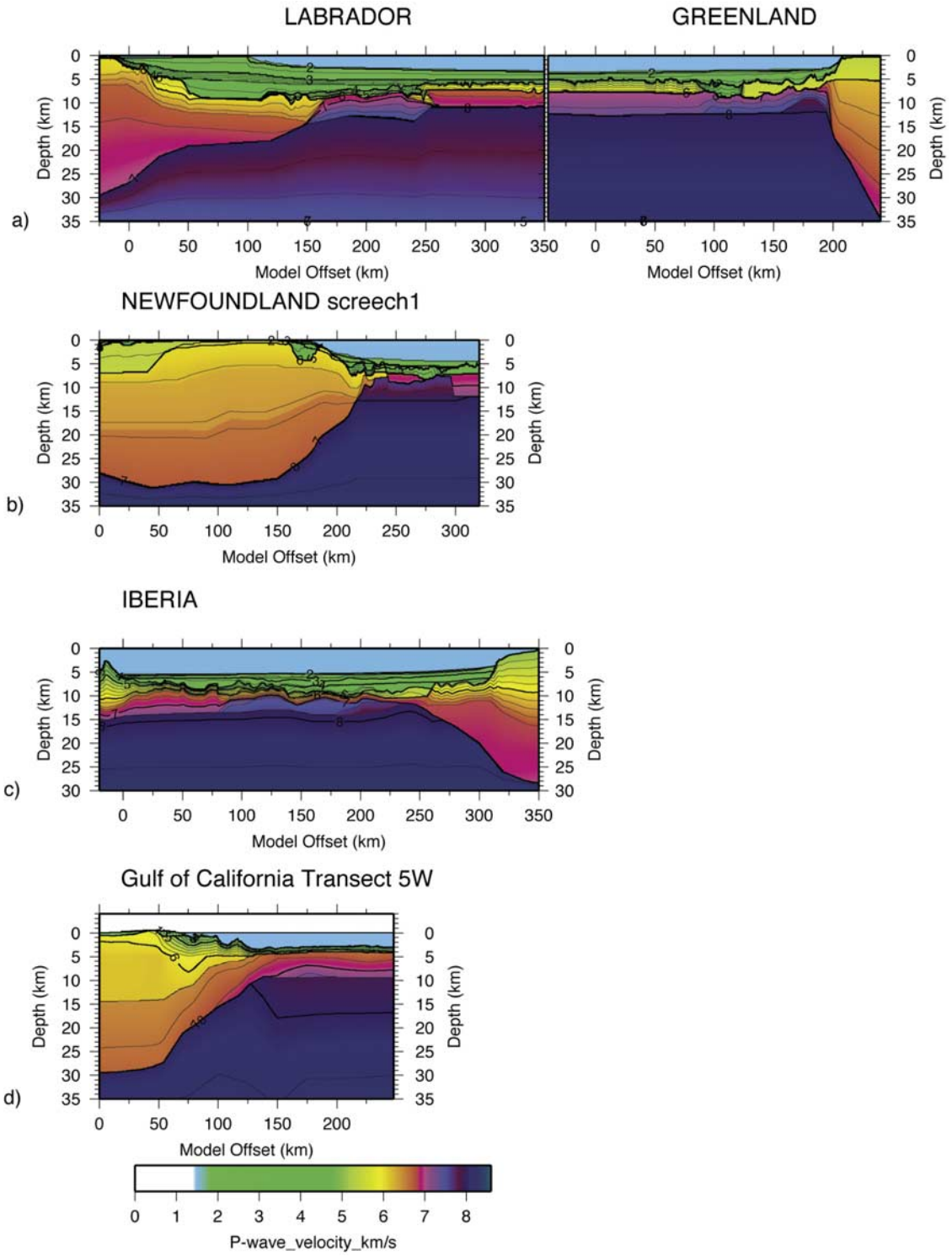

Figure 12. Comparison of transect 5W with other nonvolcanic margins from the North Atlantic and Labrador-Greenland conjugate margins. (a) Velocity model from the Labrador-Greenland conjugate margins [*Louden and Chian*, 1999; *Chian and Louden*, 1994]. (b) Velocity model from Newfoundland SCREECH1 transect [*Funck et al.*, 2003]. (c) Velocity model from Iberia transect IAM-9 [*Dean et al.*, 2000]. (d) Velocity model from the Gulf of California transect 5W.

formed by a ~75-km-wide zone of extended and block-faulted continental crust (Figure 12d), followed by typical oceanic crustal thickness and velocities, with no indication of tracts of serpentinized upper mantle. The significance of the absence of serpentinized upper mantle on transect 5W is discussed below.

[36] Continental breakup involves a combination of magmatic and tectonic processes. Tectonic models have focused

mainly on styles of extension and strength distribution [*Kusznir and Park*, 1987; *Bassi et al.*, 1993], while magmatic models depend on mantle temperature, rate and duration of rifting and initial lithospheric thickness [*Bown and White*, 1994]. The rifted margins compared in Figure 12 all share a similar initial crustal thickness and width of the extended continental crust. This suggests some similarity in the style of extension involved during rifting; relatively thin crust (<30 km) and low to intermediate mantle temperatures made the lithosphere strong and brittle, and abrupt necking took place. However, the continent-ocean transition of the rifted transects from the North Atlantic and the Labrador-Greenland conjugate margins differ substantially from that found in transect 5W in the Gulf of California. Oceanic crustal thicknesses inferred from numerical models do not vary considerably for full spreading rates between 20 and 150 mm a^{-1}, but an abrupt decrease in oceanic thickness, or melt generation, is observed for spreading rates below 15 mm a^{-1} [*Bown and White*, 1994], due to conductive heat loss of the slowly upwelling mantle. The slower spreading rates of the North Atlantic and Labrador-Greenland margins made favorable conditions for magma-starved rifting and consequently produced wider continent-ocean transition than in the southern Gulf of California. The distribution of magmatic rocks across the newly formed oceanic crust and the adjacent continental margin is controlled by the rate at which melt is produced and the ease with which it can spread through the crust [*White*, 1992]. More rapidly upwelling mantle from transect 5W had less time to lose heat by conduction and produced thicker initial oceanic crust than in the North Atlantic and Labrador-Greenland margins. A full spreading rate of ~48 mm a^{-1} in transect 5W favored sufficient melt generation to create crustal thicknesses of ~6.4 km. Oceanic crustal thicknesses at that spreading rate are in accordance with those predicted by numerical models of spreading rate vs. crustal thickness by *Bown and White* [1994]. Few observations have been made on non–end-member margins such as transect 5W in which the seismic structure of a nonvolcanic margin lacks the presence of exposed upper mantle. Thus our results support Bown and White's idea that spreading rate exerts a major control on whether nonvolcanic margins develop tracts of exposed serpentinized upper mantle [e.g., *Chian et al.*, 1995; *Whitmarsh and Sawyer*, 1996].

7. Conclusions

[37] The PESCADOR experiment provides the clearest seismic structure to date of the continent-ocean transition on the southern Gulf of California. Wide-angle data quality and ray coverage were excellent between model km 60–200, providing good velocity control across the continent-ocean transition.

[38] The oceanic crust shows little lateral variations in mean crustal thickness and mean crustal velocities, indicating a fairly constant rate of magmatic productivity since seafloor spreading started. Normal mantle temperatures (1300°C) and passive upwelling are estimated at the time seafloor spreading began.

[39] The boundary between typical continental and oceanic crust is formed by a ~75-km-wide zone of extended continental crust dominated by block-faulted basement. The crust thins from ~28 km in continental crust at model km ~40 to ~6.7 km in oceanic crust at model km ~135. The total amount of extension of the whole crust in the direction of transect 5W is estimated to be ~35 km. An excess of lower crust of up to 5 km thickness is found in the extended continental crust between model km ~85–125. Melt generated by extension of the continental lithosphere will not account for the excess of lower crust. Therefore the excess of lower crust observed is likely due to a large-scale asymmetry in the margin or by lower crustal flow.

[40] The rift architecture observed in transect 5W is in accordance with a narrow rift mode of extension, where thin crust (~28 km) and mantle temperatures of ~1300°C made the lithosphere strong and stress-bearing layers, predominately brittle, caused abrupt necking of the entire lithosphere. Following crustal extension, new oceanic crust ~6.4 km thick was formed at a rate of ~48 mm a^{-1} to accommodate plate separation.

[41] **Acknowledgments.** We thank the captain and the crew of the R/V *Maurice Ewing* and R/V *New Horizon* for their hard work during the long cruise. This work was supported by the National Science Foundation MARGINS program, grant OCE-0112152.

References

Amor, J. R. (1996), PLOTSEC: Generalized software for seismic refraction data, *LSPF Newsl. 9*, pp. 24–31, Univ. of Calgary, Calgary, Alberta, Canada.

Artemieva, I. M., and W. D. Mooney (2001), Thermal thickness of cratonic lithosphere: A global study, *J. Geophys. Res.*, *106*, 16,387–16,414.

Atwater, T. (1970), Implications of plate tectonics for the Cenozoic tectonic evolution of western North America, *Geol. Soc. Am. Bull.*, *81*, 3513–3536.

Atwater, T., and J. Stock (1998), Pacific-North America plate tectonics of the Neogene southwestern United States—An update, *Int. Geol. Rev.*, *40*, 375–402.

Axen, G. J., M. Grove, D. Stockli, O. M. Lovera, D. A. Rothstein, J. M. Fletcher, K. Farley, and P. L. Abbott (2000), Thermal evolution of Monte Blanco dome: Low-angle normal faulting during Gulf of California rifting and late Eocene denudation of the eastern Peninsular Ranges, *Tectonics*, *19*, 197–212.

Bassi, G. (1995), Relative importance of strain-rate and rheology for the mode of continental extension, *Geophys. J. Int.*, *122*, 195–210.

Bassi, G., C. E. Keen, and Potter (1993), Contrasting styles of rifting models and examples from the eastern Canadian margin, *Tectonics*, *12*, 639–655.

Behn, M. D., J. Lin, and M. T. Zuber (2002), A continuum mechanics model for normal faulting using a strain-rate softening rheology: Implications for thermal and rheological controls on continental and oceanic rifting, *Earth Planet. Sci. Lett.*, *202*, 725–740.

Blakely, R. J. (1996), *Potential Theory in Gravity and Magnetic Applications*, Cambridge Univ. Press, New York.

Bown, J. W., and R. S. White (1994), Variation with spreading rate of oceanic crustal thickness and geochemistry, *Earth Planet. Sci. Lett.*, *121*, 435–449.

Brown, H. E., W. S. Holbrook, P. Páramo, D. Lizarralde, J. Fletcher, P. Umhoefer, G. Kent, A. Harding, Gonzalez, and G. Axen (2005), Crustal structure of the southern Gulf of California, from the East Pacific rise to the Jalisco Block, *Eos Trans. AGU*, *86*(52), Fall Meet. Suppl., Abstract T33-1734.

Buck, W. R. (1991), Modes of continental lithospheric extension, *J. Geophys. Res.*, *96*, 20,161–20,178.

Canales, J. P., R. S. Detrick, S. Bazin, A. J. Harding, and J. A. Orcutt (1998), Off-Axis crustal thickness across and along the East Pacific Rise within the MELT Area, *Nature*, *280*, 1218–1221.

Chian, D., and K. E. Louden (1994), The continent-ocean crustal transition across the southwest Greenland margin, *J. Geophys. Res.*, *99*, 9117–9135.

Chian, D., and K. E. Louden (1995), Crustal structure of the Labrador Sea conjugate margin and implications for the formation of nonvolcanic continental margins, *J. Geophys. Res.*, *100*, 24,239–24,253.

Chian, D., C. Keen, and I. Reid (1995), Evolution of nonvolcanic rifted margins: New results from the conjugate margins of the Labrador Sea, *Geology*, *23*(7), 589–592.

Christensen, N. I., and W. D. Mooney (1995), Seismic velocity structure and composition of the continental crust: A global view, *J. Geophys. Res.*, *100*, 9761–9788.

Clayton, R. W., et al. (2004), The NARS-Baja seismic array in the Gulf of California rift zone, *Margins Newsl.*, *13*, 1–4.

Davis, M. J., and N. J. Kusznir (2004), Depth-dependent lithospheric stretching at rifted continental margins, in *Rheology and Deformation of the Lithosphere at Continental Margins*, edited by G. D. Karner et al., pp. 92–137, Columbia Univ. Press, New York.

Dean, S. M., T. A. Minshull, R. B. Whitmarsh, and K. E. Louden (2000), Deep structure of the ocean-continent transition in the southern Iberia Abyssal Plain from seismic refraction profiles: The IAM-9 transect at 40°20′N, *J. Geophys. Res.*, *105*, 5859–5885.

DeMets, C. (1995), A reappraisal of seafloor spreading lineations in the Gulf of California: Implications for the transfer of Baja California to the Pacific plate and estimates of Pacific-North America motion, *Geophys. Res. Lett.*, *22*, 3545–3548.

DeMets, C., and T. H. Dixon (1999), New kinematic models for Pacific-North America motion from 3 Ma to present: 1. Evidence for steady motion and biases in the NUVEL-1A model, *Geophys. Res. Lett.*, *26*, 1921–1924.

DeMets, C., R. G. Gordon, S. Stein, and D. F. Argus (1987), A revised estimate of Pacific-North America motion and implications for western North America plate boundary zone tectonics, *Geophys. Res. Lett.*, *14*, 911–914.

Detrick, R., J. Collins, R. Stephen, and S. Swift (1994), In situ evidence for the nature of the seismic layer 2/3 boundary in the oceanic crust, *Nature*, *370*, 288–290.

Dixon, T., F. Farina, C. DeMets, F. Suarez-Vidal, J. Fletcher, B. Marquez-Azua, M. Miller, O. Sanchez, and P. Umhoefer (2000), New Kinematic models for Pacific-North America motion from 3 Ma to present: 2. Evidence for a ''Baja California shear zone'', *Geophys. Res. Lett.*, *27*, 3961–3964.

Driscoll, N. W., and G. D. Karner (1998), Lower crustal extension across the Northern Carnarvon basin, Australia: Evidence for an eastward dipping detachment, *J. Geophys. Res.*, *103*, 4975–4991.

Dunbar, J. A., and D. S. Sawyer (1989), Patterns of continental extension along the conjugate Margins of the Central and North Atlantic oceans and Labrador Sea, *Tectonics*, *8*, 1059–1077.

Finlayson, D. M., C. D. Collins, I. Lukaszyk, and E. C. Chudky (1998), A transect across Australia's southern margin in the Otway basin region: Crustal architecture and the nature of rifting from wide-angle seismic profiling, *Tectonophysics*, *288*, 177–189.

Fletcher, J. M., and L. Munguía (2000), Active continental rifting in southern Baja California, Mexico: Implications for plate motion partitioning and the transition to seafloor spreading in the Gulf of California, *Tectonics*, *19*, 1107–1123.

Fletcher, J. M., B. Kohn, D. A. Foster, and A. J. Gleadow (2000), Heterogeneous Neogene cooling and exhumation of the Los Cabos block, southern Baja California: Evidence from fission-track thermochronology, *Geology*, *28*(2), 107–110.

Fletcher, J. M., J. A. Pérez-Venzor, G. Gonzalez-Barba, and J. J. Aranda-Gomez (2003), Ridge-trench interactions and the ongoing capture of the Baja California microplate—New insights from the southern Gulf Extensional Province, in *Geologic Transects Across Cordilleran Mexico, Guidebook for the Field Trips of the 99th Geological Soc. of America Cordilleran Section Annual Meeting, Puerto Vallarta, Jalisco, Mexico, March 29–31, 2003*, *Publ. Esp. 1, Field Trip 2*, pp. 13–31, Univ. Nac. Autó. de Mexico, Inst. de Geol., Mexico, D. F.

Funck, T., J. R. Hopper, H. C. Larsen, K. E. Louden, B. E. Tucholke, and W. S. Holbrook (2003), Crustal structure of the ocean-continent transition at Flemish Cap: Seismic refraction results, *J. Geophys. Res.*, *108*(B11), 2531, doi:10.1029/2003JB002434.

González-Fernández, A., J. J. Dañobeitia, L. A. Delgado-Argote, F. Michaud, D. Córdoba, and R. Bartolomé (2005), Mode of extension and rifting history of upper Tiburón and upper Delfín basins, northern Gulf of California, *J. Geophys. Res.*, *110*, B01313, doi:10.1029/2003JB002941.

Hausback, B. (1984), Cenozoic volcanism and tectonic evolution of Baja California Sur, Mexico, *Soc. Econ. Paleontol. Mineral.*, *39*, 219–236.

Holbrook, W. S., and B. Kelemen (1993), Large igneous province on the US Atlantic margin and implications for magmatism during continental breakup, *Nature*, *364*, 433–436.

Holbrook, W. S., G. M. Purdy, R. E. Sheridan, and L. Glover (1994), Seismic structure of the U.S. Mid-Atlantic continental margin, *J. Geophys. Res.*, *99*, 17,871–17,891.

Holbrook, W. S., et al. (2001), Mantle thermal structure and active upwelling during continental breakup in the North Atlantic, *Earth Planet. Sci. Lett.*, *190*, 251–266.

Hopper, J. R., and W. R. Buck (1996), The effect of lower crustal flow on continental extension And passive margin formation, *J. Geophys. Res.*, *101*, 20,175–20,194.

Karig, D. E., and W. Jensky (1972), The Proto-Gulf of California, *Earth Planet. Sci. Lett.*, *17*, 169–174.

Kelemen, B., and W. S. Holbrook (1995), Origin of thick, high-velocity igneous crust along the U.S. East Coast Margin, *J. Geophys. Res.*, *100*, 10,077–10,094.

Klein, E. M., and C. H. Langmuir (1987), Global correlations of ocean ridge basalt chemistry with axial depth and crustal thickness, *J. Geophys. Res.*, *92*, 8089–8115.

Korenaga, J., P. B. Kelemen, and W. S. Holbrook (2002), Methods for resolving the origin of large igneous provinces from crustal seismology, *J. Geophys. Res.*, *107*(B9), 2178, doi:10.1029/2001JB001030.

Kusznir, N. J., and R. G. Park (1987), The extensional strength of the continental lithosphere: Its dependence on geothermal gradient, and crustal composition and thickness, in *Continental Extensional Tectonics*, edited by M. P. Coward, J. F. Dewey, and P. L. Hancock, *Geol. Soc. Spec. Publ.*, *28*, 35–52.

Kusznir, N. J., G. Marsden, and S. S. Egan (1991), A flexural-cantilever simple-shear/pure-shear model of continental lithosphere extension: Applications to the Jeanne d'Arc Basin, Grand Banks and Viking Graben, North Sea, in *The Geometry of Normal Faults*, edited by A. M. Roberts, G. Yielding, and B. Freeman, *Geol. Soc. Spec. Publ.*, *56*, 41–60.

Langmuir, C. H., E. M. Klein, and T. Plank (1992), Petrological constraints on melt formation and migration beneath mid-ocean ridges, in *Mantle Flow and Melt Generation at Mid-Ocean Ridges*, *Geophys. Monogr. Ser.*, vol. 71, edited by J. Phipps Morgan, D. Blackman, and J. L. Sinton, pp. 183–280, AGU, Washington, D. C.

Lavier, L. L., and G. Manatschal (2006), A mechanism to thin the continental lithosphere at magma-poor margins, *Nature*, *440*, 324–328.

Lister, G. S., M. A. Etheridge, and A. Symonds (1986), Detachment faulting and evolution of passive continental margins, *Geology*, *14*, 246–250.

Lizarralde, D., and W. S. Holbrook (1997), Structure and early thermal evolution of the U.S. Mid-Atlantic margin, *J. Geophys. Res.*, *102*, 22,855–22,875.

Lizarralde, D., G. J. Axen, J. M. Fletcher, A. G. Fernandez, W. S. Holbrook, A. J. Harding, G. M. Kent, and Umhoefer (2003), Crustal structure and rift evolution across the Guaymas Basin, Gulf of California, *Eos Trans. AGU*, *84*(46), Fall Meet. Suppl., Abstract T31E-0886.

Lizarralde, D., et al. (2007), Variations in styles of rifting in the Gulf of California, *Nature*, *448*, 466–469.

Lonsdale, P. (1989), Geology and tectonic history of the Gulf of California, in *The Geology of North America*, vol. N, *The Eastern Pacific Ocean and Hawaii*, edited by E. L. Winterer, D. M. Hussong, and R. W. Decker, pp. 499–521, Geol. Soc. of Am., Boulder, Colo.

Louden, K. E., and D. Chian (1999), The deep structure of non-volcanic rifted continental margins, *Philos. Tran. R. Soc. London, Ser. A*, *357*, 767–804.

McKenzie, D. (1978), Some remarks on the development of sedimentary basins, *Earth Planet. Sci. Lett.*, *40*, 25–32.

McKenzie, D., and M. J. Bickle (1988), The volume and composition of melt generated by extension of the lithosphere, *J. Petrol.*, *29*, 625–679.

Michaud, F., et al. (2006), Oceanic-ridge subduction vs. slab break off: Plate tectonic evolution along the Baja California Sur continental margin since 15 Ma, *Geology*, *29*(1), 13–16, doi:10.1130/G22050.1.

Mutter, J. C., M. Talwani, and L. Stoffa (1982), Origin of seaward-dipping reflectors in oceanic crust off the Norwegian margin by subaerial seafloor spreading, *Geology*, *10*(7), 353–357.

National Geophysical Data Center (1999), Mexico gravity data (MEXICO97), NOAA, U.S. Dep. of Commer., Silver Spring, Md.

Oskin, M., J. M. Stock, and A. Martín-Barajas (2001), Rapid localization of Pacific-North America plate motion in the Gulf of California, *Geology*, *29*(5), 459–462.

Pérez-Gussinyé, M., and T. J. Reston (2001), Rheological evolution during extension at passive non-volcanic margins: Onset of serpentinization and development of detachments to continental breakup, *J. Geophys. Res.*, *106*, 3961–3975.

Pérez-Gussinyé, M., C. R. Ranero, T. J. Reston, and D. Sawyer (2003), Mechanisms of extension at nonvolcanic margins: Evidence from the Galicia interior basin, west of Iberia, *J. Geophys. Res.*, *108*(B5), 2245, doi:10.1029/2001JB000901.

Péron-Pinvidic, G., G. Manatschal, T. A. Minshull, and D. S. Sawyer (2007), Tectonosedimentary evolution of the deep Iberia-Newfoundland margins: Evidence for a complex breakup history, *Tectonics*, *26*, TC2011, doi:10.1029/2006TC001970.

Pickup, S. L., R. B. Whitmarsh, C. M. R. Fowler, and T. J. Reston (1996), Insight into the nature of the ocean-continent transition from a deep multichannel seismic reflection profile, *Geology*, *24*(12), 1079–1082.

Pinheiro, L. M., R. B. Whitmarsh, and R. Miles (1992), The ocean-continent boundary off the western continental margin of Iberia-II. Crustal structure in the Tagus Abyssal plain, *Geophys. J. Int.*, *109*, 106–124.

Reid, I. (1994), Crustal structure of a nonvolcanic rifted margin east of Newfoundland, *J. Geophys. Res.*, *99*, 15,161–15,180.

Reston, T. (2007), Extension discrepancy at North Atlantic nonvolcanic rifted margins: Depth-dependent stretching or unrecognized faulting?, *Geology*, *35*(4), 367–370, doi:10.1130/G23213A.1.

Sallares, V., and P. Charvis (2003), Crustal thickness constraints on the geodynamic evolution of the Galapagos Volcanic Province, *Earth Planet. Sci. Lett.*, *214*(3–4), 545–559.

Sallarès, V., P. Charvis, E. R. Flueh, and J. Bialas (2003), Seismic structure of Cocos and Malpelo Volcanic ridges and implications for hot spot-ridge interaction, *J. Geophys. Res.*, *108*(B12), 2564, doi:10.1029/2003JB002431.

Sawlan, M. G. (1991), Magmatic evolution of the Gulf of California rift, *AAPG Mem.*, *47*, 301–369.

Shillington, D. J., W. S. Holbrook, H. J. A. Van Avendonk, B. E. Tucholke, J. R. Hopper, K. E. Louden, H. C. Larsen, and G. T. Nunes (2006), Evidence for asymmetric nonvolcanic rifting and slow incipient oceanic accretion from seismic reflection data on the Newfoundland margin, *J. Geophys. Res.*, *111*, B09402, doi:10.1029/2005JB003981.

Stock, J., and M. J. Lee (1994), Do microplates in subduction zones leave a geological record?, *Tectonics*, *13*, 1472–1487.

Sutherland, F. H., A. J. Harding, G. M. Kent, D. Lizarralde, W. S. Holbrook, J. M. Fletcher, A. Gonzalez-Fernandez, P. Umhoefer, and G. J. Axen (2004), Continental rifting across the Alarcon Basin, Gulf of California, *Eos Trans. AGU*, *85*(47), Fall Meet. Suppl., Abstract T33C-1401.

ter Voorde, M., R. T. van Balen, G. Bertotti, and S. A. L. Cloething (1998), The influence of a stratified rheology on the flexural response of the lithosphere to (un)loading by extensional faulting, *Geophys. J. Int.*, *134*, 721–735.

Umhoefer, P. J., R. J. Dorsey, and P. Renne (1994), Tectonics of the Pliocene Loreto basin, Baja California Sur, Mexico, and evolution of the Gulf of California, *Geology*, *22*(7), 649–652.

Umhoefer, P. J., R. J. Dorsey, S. Willsey, L. Mayer, and P. Renne (2001), Stratigraphy and Geochronology of the Comondú Group near Loreto, Baja California Sur, Mexico, *Sediment. Geol.*, *144*, 125–147.

White, R. S. (1992), Crustal structure and magmatism of North Atlantic continental margins, *J. Geol. Soc. London*, *149*, 841–854.

White, R. S., and D. McKenzie (1989), Magmatism at rift zones: The generation of volcanic Continental margins and flood basalts, *J. Geophys. Res.*, *94*, 7685–7729.

Whitmarsh, R. B., and D. S. Sawyer (1996), The ocean/continent transition beneath the Iberia Abyssal Plain and continental-rifting to seafloor-spreading processes, *Proc. Ocean Drill. Program Sci. Results*, *149*, 713–733.

Zelt, C. A., and R. B. Smith (1992), Seismic inversion for 2-D crustal velocity structure, *Geophysics. J. Int.*, *108*, 16–34.

G. Axen, Department of Earth and Environmental Science, New Mexico Institute of Mining and Technology, Socorro, NM 87801, USA.

H. E. Brown and W. S. Holbrook, Department of Geology and Geophysics, University of Wyoming, Laramie, WY 82071, USA.

J. Fletcher and A. Gonzalez, Department of Geology, CICESE, Ensenada, Baja California, Mexico.

A. Harding and G. Kent, Scripps Institution of Oceanography, University of California, San Diego, 9500 Gilman Drive, La Jolla, CA 92093-0225, USA.

D. Lizarralde, Department of Geology and Geophysics, Woods Hole Oceanographic Institution, Woods Hole, MA 02543-1541, USA.

P. Páramo, BP Exploration Operating Company Ltd., Chertsey Road, Sunbury-on-Thames TW16 7LN, UK. (txominparamo@gmail.com)

P. Umhoefer, Department of Geology, Northern Arizona University, Flagstaff, AZ 86011, USA.